STRUCTURE PROPERTY RELATIONSHIPS OF CARBOHYDRATE/PROTEIN BASED BIOMATERIALS

By

JOHN STANTON

A thesis submitted to the

Graduate School-Camden

Rutgers, The State University of New Jersey

In partial fulfillment of the requirements

For the degree of Master of Science

Graduate Program in Chemistry

Written under the direction of

Dr. David Salas-de la Cruz

and approved by

_____

David Salas-de la Cruz, Ph.D.

_____

George Kumi, Ph.D.

_____

Xiao Hu, Ph.D.

Camden, New Jersey

May 2017

THESIS ABSTRACT

Structure Property Relationships of Carbohydrate/Protein based Biomaterials

by JOHN STANTON

Thesis Director:

Dr. David Salas- de la Cruz

Cellulose and silk blended biomaterial films were regenerated from ionic liquid solutions and investigated to characterize and understand the effect of inter- and intra-molecular interactions upon the structure, morphology and thermal properties. The investigation focuses on studying these effects as a function of silk to cellulose concentration and as a function of ionic liquid type with a constant silk to cellulose concentration. Various characterization techniques were used to characterize structural, morphological and thermal properties: Fourier transform infrared spectroscopy (FTIR), scanning electron microscopy (SEM), thermal gravimetric analysis (TGA), differential scanning calorimetry (DSC) and X-ray scattering. The data shows that the inter- and intra-molecular interactions allow for different structures to be formed. The results showed that the cellulose microcrystalline structure and β-sheets from the silk can be disrupted by inter- and intra-molecular hydrogen bonds and lead to the formation of intermediate semicrystalline or amorphous structures. These various techniques provide evidence that suggest the hydrogen bonds between the β-sheets and the glucose units in the cellulose chains control the thermal and structural properties of the blended films, changing the morphology and physicochemical properties. The type of structure obtained can be

modified by the type of ionic liquid, especially the type of anion used. A large anion with increased interactions controls the thermal properties and the crystallinity of the film.

Dedications

I would like to dedicate this thesis to my family for their support throughout my entire academic career. The encouragement of my parents John and Marguerite Stanton and their unconditional love that allowed me to make it this far. My grandparents Angelo Silineo and Shirley Stanton for encouraging me to pursue my dream of higher education. All of them are special to me and I am very lucky to have such great people in my family.

Acknowledgements

To Dr. Salas, I would like to thank you for allowing me to be a part of your lab team. I do not think I can express my gratitude enough to you for helping me on this long road we have been on together. You helped me throughout my academic career with your enthusiasm and gave me the tools to succeed. The patience you had with me and the guidance you have given me during the project has allowed both of us to come so far. Thank you for teaching me and giving me real world skills that will benefit me in my future endeavors, where ever they might be. I like to think you helped me grow as a person and become the best I can be.

To Mrs. Craig, I would like to express how grateful I am for all the support you have given me throughout the years. As an undergraduate you supported me throughout my class work and always had time to answer any questions I had about my classes. You have always been there when I needed someone to talk especially when I started stressing out. You allowed me to be a part time lecturer when I made it to the graduate program, that opened a whole new opportunity in career choices that I never thought about. You always encouraged and motivated me to be the best person I can be. I am proud to help share the knowledge you bestowed me with future students coming to Rutgers.

Table of Content

List of Tables

List of Figures

Chapter 1

Introduction

1.0 Introduction

1.1 Biomaterials

Biomaterial science is a growing field that focuses on studying and understanding how the inter- and intra-molecular interactions of materials affect the material physicochemical properties. The interactions directly affect the morphology and subsequently the cell-biomaterials interactions, to interact advantageously with biological systems to aid in human health. The term biomaterial refers to a nonviable material used in medical textile devices to interact with a biological system. However, this definition can be broadened to encompass a variety of applications, such as the development of scaffolds for cell proliferation, assays for blood proteins, and in the development of equipment for biotechnological applications [1]. This definition can also include tissue engineering, the creation of artificial organs, and applications in the energy and environmental sectors [1-3]. One of the advantages of biomaterials is that their properties are tunable and can be changed depending on the material composition. Biomaterials can be divided into two groups: artificial materials and natural materials [4]. Natural materials, as the name reflects, use natural polymers, for example cellulose, proteins, cultured cells, and preserved tissues. Artificial materials can be broken down into organics, synthetic polymers, and inorganic materials, and metals [4]. Materials from both groups can be combined to make a hybrid biomaterial that be used in any of the mentioned applications, as the properties depend on their biocompatibility and the targeted goals [1].

Biocompatibility is essential for the creation of useful biomaterial applications in the medical sector. The term biocompatibility is defined as "the ability of a material to perform an appropriate host response in a specific application" [1]. This leads to studies investigating the *in-vitro* and *in-vivo* processes for cell, materials, metabolic, and biomechanical conditions of regenerated tissues [1]. Bio-adaptability is an important subset of biocompatibility. The biocompatibility of a biomaterial to a tissue depends on the

material's mechanical, morphological, volumetric and biochemical properties [4]. Thus, the morphological and interfacial properties of a material are especially important for determining its biocompatibility [4]. Biocompatible materials are generally categorized into 3 different classes. Class I contains materials that do not make any direct contact with tissues. Class II deals with materials that make contact with the tissues at certain intervals or instantly.

Class III, the most significant biomedical classification, has constant interaction with the tissues. Class III can be further parsed into three more categories: bioinert, bioactive, and biodegradable. Bioinert indicates that a material has no immunological host reactions but its structures do remain in the host. A bioactive material mimics the properties of natural tissues, acting as a biological function. Biodegradable materials are absorbed into the body and are replaced by the regenerated tissue [4].

The medical community more frequently uses this terminology when describing materials than chemists, but these features are very important to understand the overall purpose and demand of biomaterial research. Natural biomaterials that can be used as scaffolds for tissue engineering applications provide excellent biocompatibility with minimal immune response following implantation. In addition, our ability to tune their morphological and physical properties enables us to enhance their interactions with cells, and to control the cellular behavior [5]. This investigation will explore the inter- and intra-molecular interactions of natural biomaterials in order to study and investigate their morphological, thermal and physical properties.

1.2 Polysaccharides

Despite being an underutilized biomaterial component, polysaccharides are gaining recognition as a viable material for biomaterial research. Polysaccharides have many favorable properties for medical applications (tissue research and engineering) including positive cell signaling, automated synthesis of oligosaccharides that are biologically active, and excellent biodegradability [6]. A major advantage in using polysaccharides is that they can form hydrogels that can be used in biological systems. The formation of hydrogels is dependent on the type of monosaccharides comprising the polysaccharide [6]. The formation usually involves hydrogen or ionic bonding in order for gel formation to occur.

Polymeric carbohydrates are made of long chains of monosaccharides, held together by glycosidic linkages. Depending on their structure, these macromolecules have various properties that are affected by the monosaccharide [7]. Some of these changes in properties range from solubility in water to the ability of a crystalline structure to be formed. Polysaccharides are heterogeneous and contain small changes to the repeating units. These repeating units usually consist of more than ten monosaccharides units [7]. Polysaccharides that are heteropolysaccharides (such as hemicellulose) are multifaceted due to their varying monosaccharides composition, and it is this complexity that leads to different formations and structures that can be tuned for biomedical applications. Natural polymers are desirable biomaterials because of their biocompatibility, biodegradability, non-toxic nature and relatively inexpensive price.

1.3 Carbohydrates

Carbohydrates are classified based on their degree of polymerization. Carbohydrates are the most abundant molecules in nature and include sugar, cellulose, and starch. The empirical formula for carbohydrates is $C_mH_{2n}O_n$, where n is less than or equal to three, and the name "carbohydrates" derives from the fact that carbons interact with water through dehydration reactions to form carbohydrate molecules [8].

Typically, carbohydrates are used to provide energy for cellular processes and are very important for all living things. For example, the oxidation of glucose results in the formation of ATP to fuel the cellular activity [8]. The glucose monomer can be made into many different macromolecules. A common one, that will be discussed more in depth in a later section, is cellulose found in plant cell walls. Glycogen is another common macromolecule produced from glucose and is distinguished due to the glycosidic bonds attached between the glucose monomers [8].

The main factor in determining the different carbohydrates interactions comes from the carbohydrates' differing backbone structure monomers, the structural characteristics of the molecules, type of linkages, and the amount or lack of branching [9]. Carbohydrates as a starting material can be used to design polymers with tunable properties, making the polymers more versatile. The ability of the monomer to copolymerize allows for desired

functional groups to be added, thereby changing the properties of polymers[3]. This allows for a more diverse range of application that can be applied to current polymers.

1.4 Cellulose

Cellulose is a carbohydrate and organic compound with the molecular formula of $(C_6H_{10}O_5)_n$. It is one of the most abundant materials in the world and is found as cellulose I (Iα or Iβ) [10]. Cellulose Iα is found in the majority of algae and bacteria, while a majority of Iβ is found in plants [11]. Cellulose can be found in 3 forms other than cellulose I (i.e. cellulose II , III, and IV). Cellulose II-IV contain other molecular configurations than cellulose I, with cellulose II being a meta stable form of cellulose occurring from regeneration. Cellulose III and IV are produced from other chemical treatments [12, 13]. Cellulose is a linear polysaccharide containing both crystalline and amorphous regions, and its β(1-4) glycosidic bonds enable strong intramolecular and intermolecular hydrogen bonding as shown in **Figure 1.1**. It has many desirable properties including its renewability from plants and bacteria [14].

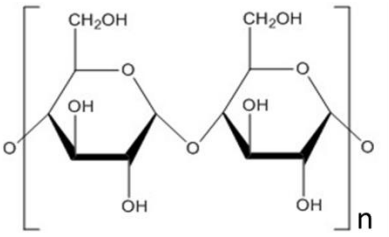

Figure 1.1. *An example of a carbohydrate structure of α-cellulose, showing the glycosidic bonds and the hydroxyl groups.*

The properties of cellulose depend on the degree of polymerization since the number of glucose monomer units (the chain length) result in different properties. The cellulose found in plant fibers is a hierarchical structure. Cellulose has both anhydro glucose units and a hemiacetal hydroxyl group with a reducing end. This causes cellulose chains to pack in a parallel pattern that allows for the crystallization of fibrils [11]. In plants cellulose exists in many different levels, from a single chain to a microfibril to cellulose fibers. This is believed to be a result of cell growth, which causes the microfibrils to separate into smaller microfibrils and interact with other molecules [11]. Cellulose is

one of the most produced biopolymers in the world, with $7.5x10^8$ tons produced yearly [15].

With this success in cultivation, cellulose can be commercially used in many fields such as the fields of materials, energy, food industry and personal products. Cellulose has advantageous properties such as biodegradability, biocompatibility, non-toxicity, hydrophilicity, thermal stability and chemical stability [15]. The one major disadvantage of cellulose is that it has high thermal stability up to 270 ˚C, and it is insoluble in typical solvents [16]. Its semicrystalline structure and its hydrogen bonding network makes its processability difficult. Along with these conditions, it forms different conformations depending on the condition of the surrounding environment, such as pH, temperature and ionic strength [15, 17]. In this case, a blend must be made by using naturally occurring biopolymers to greatly improve its properties such as the thermal stability, morphological, and mechanical properties of the cellulose material.

1.5 Natural Proteins

Another type of polymer of interest for biomaterial research are natural proteins. Structural proteins are of interest because their structural and bioactive properties have evolved to adapt well to a given environment. Structural proteins are characterized by the primary amino acid sequences that are repeated within the proteins [18]. Naturally silks are a type of polymer protein that are produced by a variety of insects; silkworms, spiders, flies, and scorpions [19]. These proteins are produced from glands that synthesize the silk-like material, which then goes through the lumen of the gland to produce the fully developed protein fibers. The final silk material is then stored in special glands for later secretion [19]. Because the sources of silks are diverse, the structural composition and the properties of the silk also vary to fit the needs of the insect that produces it. In some cases, cocoons are produced for reproduction while other insects use it as a way of capturing prey, such as a web. The proteins of silk allow for self-assembly, similar to cellulose's structural hierarchy [18]. Fibrous proteins such as these have homogeneity in their secondary structures, either in the α-helices or the β-sheets [19]. In these biopolymers, certain interactions (such as van der Waals, hydrogen bonding, and hydrophobic/hydrophilic interactions with functional groups) occur [20]. The strong mechanical properties of

proteins give them good potential as viable biomaterials for biomedical applications, where they can be used as scaffolding for tissue engineering and controlled drug delivery.

1.6 Bombyx Mori Silk

The focus on a natural protein in this study will concentrate on silk, specifically the Bombyx Mori silk from silk worms, which has been used in the textile industry for thousands of years [20]. The silk worms are domesticated and easy to maintain through a diet of mulberries which leads to a high yield in cocoon production [19]. The larvae of the silkworms are easy to maintain in high concentration due to their small size and high reproduction rate [19]. The silk is produced originally as a silk I material, meaning that the fiber is water soluble and is in a glue-like form called sericin. The fiber is then converted into the silk II structure which is water insoluble [20]. The silk material forms insoluble crystalline regions of stacked β-sheets in the fiber due to its primary structure's configuration which is mainly comprised of a highly repetitive pattern of the amino acid sequence $[GAGAGS]_n$ as observed in **Figure 1.2** [18]. This allows for physical crosslinking to occur with the silk material that enables the β-sheets to form a highly stable structure [21]. The β-sheets are in specific anti-parallel arrangements, a feature that is of interest in the biomedical field. The β-sheet crystals of Mori silk can be made into robust biomaterials for tissue regeneration and drug delivery applications [18]. However, the difficulty in using silk for biomaterials is the dissolution process, as the Mori silk contains a strongly hydrogen bonded network and hydrophobic regions that resists dissolution. Some studies have shown that the Mori silk will interact with polysaccharides because of the hydrophobic-hydrophobic interactions [22]. The properties of the silk can be used in combination with other polymers to improve material properties.

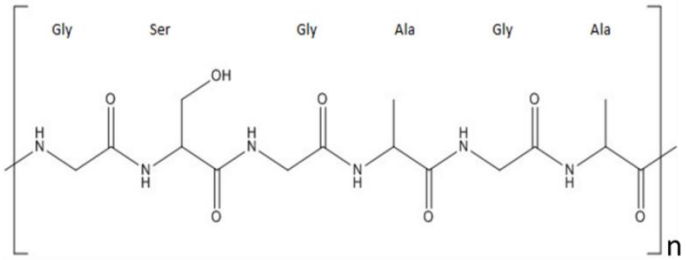

Figure 1.2. The *structure of the natural polymer Bombyx Mori Silk from silk worms showing the principle components in the polymer in its entirety.*

1.7 Dissolution

As previously stated in sections 1.4 and 1.6, the solubility of a material is often problematic as a poor solvent will affect the miscibility of the protein-polysaccharide film. Most organic solvents that are used in industry are unsuitable, as they alter the molecular weight of the protein material during the chemical processing [23]. The toxicity of many organic solvents to the environment, unwanted side reactions, and the explosive hazards and flammability make these solutions undesirable [24]. The dissolution process also has the additional problem of solvent recovery, which then creates consequences such as high maintenance cost and continual production of the solvent [25]. Because the solvents must be continuously produced, consistency of solvent material may be difficult to achieve, and the wanted derivation of solvent may not be generated at each production [26]. The high temperatures necessary to make commonly used cellulose films makes them a disadvantageous option because the high heat degrades the solutes to a point where all material is wasted [25]. Also, a poor solvent that does not completely dissolve the given solutes will affect the miscibility, causing issues with the mechanical properties of the blended samples [23]. A possible solution is to use a solvent such as ionic liquids to produce blended materials.

1.8 Ionic Liquids

Ionic liquids are organic salts that are liquid at or near room temperature, having a melting point at or below 100 °C [24]. Unlike other organic compounds, ionic liquids (1) do not suffer from poor liquid range, (2) are free from the effects of vapor pressure, (3) are easy to recycle, (4) have a tunable structure, (5) are chemically stable, and (6) are

nonflammable [11, 14, 24, 26]. An ionic liquid structure is composed of a cation and an anion. Typically, ionic liquids have a bulky asymmetric cation that interacts with a weakly coordinated anion; this interaction allows for the ionic liquid to remain a liquid near room temperature [24, 26]. The functional groups of the cation allow for variation to occur within the structure, and this allows for certain lengths or branching structures based on the ionic chains. The possibilities of having multiple types of anions and cations allow for tunability to occur during the dissolving process with the material(s). The cation facilitates interactions through hydrogen bonding, hydrophobic interactions, or even van der Waals interactions [11]. The anion will disrupt the hydroxyl groups by disrupting the naturally occurring hydrogen bonding networks via the steric hindrance of the anion and the charge density [11]. Another benefit of ionic liquids is their recoverability, since they are water-soluble and can be recollected during the coagulation phase. Because they can be recovered, ionic liquids are also considered renewable solvents and therefore greatly reduce waste [14, 24]. Finally, the properties of ionic liquids have an overall effect of preventing changes in the degree of polymerization of selected natural biomaterials in the solution.

1.9 Imidazolium Ionic Liquids

The ionic liquids used in this study are those that have successfully dissolved either the silk protein or cellulose in previous studies [14, 19, 23, 25, 27]. The ionic liquids of focus here will be imidazolium core based, as they possess a charge rich core [28]. The imidazolium ring is a five-membered ring that consists of carbon and nitrogen double bonds with a positive charge. Typically, imidazolium rings also have a side chain group attached. The imidazolium ring allows for different alkyl chain lengths to be used on the cation. The cation charge has minor influences on the viscosity and thermal properties of the ionic liquid [28]. The thermal properties are based on van der Waals forces and electrostatic forces. These forces are determined by the hydrogen bond interactions and symmetry of the sample [28]. The cations' symmetry is of importance as it allows for thermal stability, depending on the size of the chains. Although the cation has a minor role in the interactions, the imidazolium ring has hydrogen bonding properties that are more significant for the ionic liquid's overall interaction behavior. The anion's influence is

important as it allows for the hydrogen bonding to occur between the halides, causing aromatic π-stacking interactions between the imidazolium cores [28]. The anion's disruption allows for new interaction forces to occur, with these new interactions depending on the type of functional group in the anion or cation.

The ionic liquids that will be studied are 1-allyl-3-methylimidazolium chloride (AMIMCl), 1-butyl-3-methylimidazolium chloride (BMIMCl), 1-ethyl-3-methylimidazolium chloride (EMIMCl), 1-ethyl-3-methylimidazolium acetate (EMIMAc), 1-butyl-3-methylimidazolium bromide (BMIMBr), and 1-butyl-3-methylimidazolium methane sulfonate ($BMIMMeSO_3$); structures are shown in **Figure 1.3**. The cations that were chosen are those considered to be the best to use for the dissolution process of cellulose and proteins [28]. These ionic liquids where chosen due to their similarities, allowing for more comparability. This is to study the difference in the ionic liquids and how their properties change based on the structures in order to evaluate the hydrogen bonding disruption and understand their interactions with the natural biomaterials. The hydroxyl groups of the cellulose and the silk should become disrupted in each of the ionic liquids [27, 28]. For example, the AMIMCl contains a double bond in the functional side chain, causing reduced viscosity of the ionic liquid and enhancing dissolution. The chloride anion is one of the most promising anions, and is one of the more commonly used anions for the dissolving process because of its interactions with the hydroxyl groups [25, 27, 28]. In the EMIMAc, the acetate anion is another commonly used anion that forms covalent bonds and also influences the hydroxyl groups [28, 29]. The acetate anion allows for a greater concentration of material to dissolve in the ionic liquid [29]. The bromide anion seen in the BMIMBr is used to compare the different halides as the bromide is a larger anion compared to the chloride, thus it will have more electrons to interact with. The $BMIMMeSO_3$ is a lesser studied ionic liquid, but has a resonance structure between the three oxygens, effecting the stability and structure of the blended film.

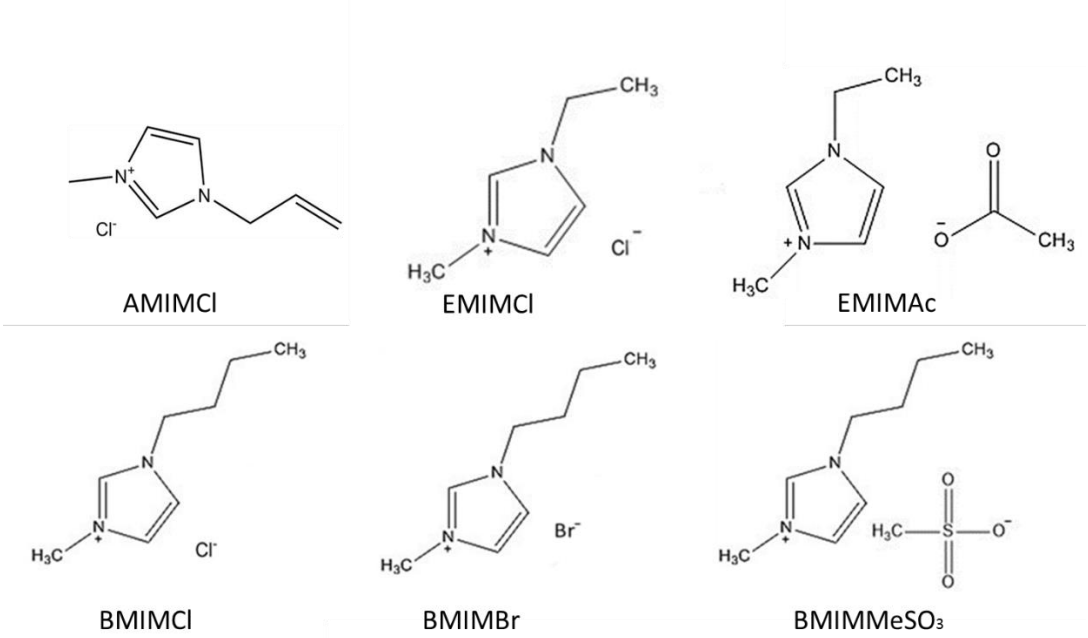

Figure 1.3. *Ionic liquid structures with cation base of methylimidazolium. Varying functional groups on the cation and varying anions are shown to allow for understanding and making comparisons.*

1.10 Goals

The known research between the cellulose and protein materials allow for a starting point to make assumptions about the interactions between the ionic liquid and the natural polymers (cellulose and silk). Most of the research has been done on the individual components, creating a polymer film with either silk or cellulose [14, 25, 28, 30]. The issue with this approach is that there is now limited information on the interactions of blended films made in ionic liquids with two components. The inability to predict the relationship between molecular interactions and spatiotemporal structures poses a significant hurdle preventing the rapid development and utilization of blended protein-polysaccharide composites seen in the proposed **Figure 1.4**. The goal of the experimentation is to understand the effects and morphological changes that are occurring in the blended films. The experiments in the following chapters will investigate the interactions between the blended film's components by observing and comparing topological patterns, thermal properties and inter- and intra- molecular morphology that result from varying

concentrations of silk and cellulose. In addition, these properties will be investigated by comparing similar concentrations of silk and cellulose as a function of the type of ionic liquid. This gives insight into how the ionic liquid, with its specific cation and anion, influences the physicochemical properties of the blended films.

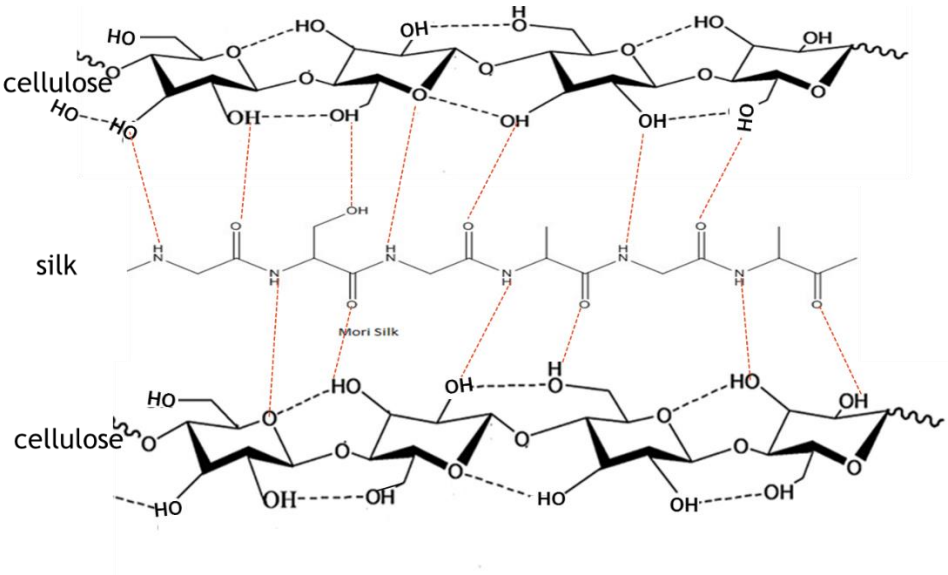

Figure 1.4 *The proposed interaction through the disruption of hydrogen bonding and the reforming of the hydrogen bonding networks.*

Chapter 2

Structure-Property Relationships of Blended Polysaccharide and Protein Biomaterials in 1-Ally-3-Methylimiadozolium Chloride

2.1 Introduction

A biomaterial is defined as a material that is crafted to interact with biological systems. Biomaterials derived from natural products have been of great interest in recent decades due to their low cost, biocompatibility, and tunable morphological and physical properties. Biomaterials research is currently a primary focus in modern technology and has led to new developments in the medical, environmental and energy sectors [2]. Currently, the medical community is exploring regenerated biomaterials with tunable properties that have minimally harmful bodily interactions.

Cellulose, a biomaterial with minimally harmful bodily interactions, is a promising candidate for medical applications and has been successfully regenerated for use in biomaterial applications for the last decade [18, 31]. The interest in cellulose as a resource derives from the fact that it is one of the most abundant materials in the world, found in nature as cellulose I (I_α or I_β) [10]. Regenerated cellulose exhibits cellulose II, amorphous and intermediate forms [32-34]. Cellulose, a polymer of glucose, is a linear polysaccharide containing both crystalline and amorphous regions that is capable of forming strong intramolecular and intermolecular hydrogen bonding [10, 13]. Over time, nature has imbued polysaccharides with varied interwoven multi-structural properties and multifunctional biological matrices that exhibit different material properties [12, 35, 36]. As seen in previous studies, cellulose is known to have high stiffness, poor solubility, and meager processability [12]. However, the most important feature of a biopolymer is its response to environmental changes. As a biopolymer, cellulose is a molecule characterized by a large molecular weight and an ability to adopt different conformations depending on the conditions of the surrounding environment, such as pH, temperature and ionic strength [17]. Consequently, the material properties of cellulose can be tuned by environmental changes and by the interaction with other materials. In this case, if a blend was produced using naturally occurring biopolymers, which would greatly improve biodegradability,

thermal stability and mechanical properties, then the cellulose material properties could be improved.

One of the best candidates for blending cellulose is the *Bombyx Mori* silk, a natural silk protein that has been used as a textile material for centuries. Mori silk has many desirable properties, such as high flexibility and high tensile strength. The silk fibroin proteins are synthesized in the glands of silkworms. Generally, a single silk thread consists of two fibroin protein fibers coated by sericin proteins. Mori silk fibroin fibers are made of thousands of parallel fibrils consisting of repetitive amino acid sequences of $(GAGAGS)_n$, that can form insoluble stacked β-sheets crystallites in the fiber. Due to large scale cultivation of domestic *Bombyx mori* silkworms, Mori silks could be a viable, green substitute for biomedical materials. Mori silk has many advantages, such as good biocompatibility, tunable degradation rate, abundance from nature or cultivation, and good structural properties and flexibility. When induced by methanol, low pH, sonication or heat, regenerated Mori silk materials can obtain a high content of β-sheet crystals [22]. With these crystals, Mori silk can be made into robust materials for various biomedical fields, such as tissue regeneration and drug delivery.

Blending allows for specific ratios to be produced, which introduces a technological advantage of creating a material that can be tunable with varying properties. Blending allows for improved material physicochemical properties and the ability to easily process material per the necessary requirements. For this natural biopolymer study, the focus is to investigate the interactions of polysaccharide and protein mixtures. Studies have shown that proteins strongly interact with polysaccharides through hydrophobic-hydrophobic interactions and electrostatic interactions [22]. These two types of interactions play a significant role in the formation and stability of a polysaccharide-protein matrix. Therefore, a way to enhance the material properties of a protein blend would be to combine the protein components with polysaccharide polymers. Polysaccharides are typically hydrophilic in nature and would control the aqueous phase rheology, meaning the thickening and the gelling, as they act as a stabilizing agent for the polysaccharide-protein matrix [3, 22, 37-39]. For this study, cellulose was used as the polysaccharide of choice. Cellulose is paramount, for it has desirable properties for a protein blend film. Combining cellulose with silk will allow for new material properties to correct the poor properties of regenerated

protein-only based films (*e.g*. relatively low degradation temperature). The use of polysaccharide-protein composites as biomaterials can lead to improved materials for the production of artificial tissues, organs, and as a coating for implants in the future.

In the process of biofilm production, there is another important consideration, the solvent. Solvents are essential, for they are the driving force for the dissolution of the cellulose and silk protein. A poor solvent will significantly affect the miscibility of polysaccharides-protein films and reduce the mechanical properties of the blends [40]. In addition, many organic solvents will heavily destroy the original molecular weight of protein materials such as silks [41]. In this investigation, an ionic liquid (IL) will be used and applied to optimize the tuning of the final material properties. Ionic liquids have been used to dissolve both cellulose and silk successfully without changing its molecular weight [30, 42]. Ionic liquids, also known as molten salts, are liquid state salts with melting points below water [43]. Ionic liquids have a combination of properties superior to typical solvents such as, negligible volatility, reusability, non-flammability, high thermal stability, and high conductivity. They have an advantage over organic solvents as they do not lead to unwanted side products and are reusable, and these properties make them a useful green alternative [43-46]. The composition of an ionic liquid is important because it contains both a bulky asymmetric cation and a weakly coordinated anion [47]. The mechanism of dissolution is the ability of the ionic liquid's anion to form hydrogen bonding with the hydroxyl groups, disrupting the naturally occurring hydrogen bonding network that is seen in cellulose crystals [11]. The same reasoning is also observed with the dissolution of *Bombyx Mori* silk [30].

In this study, the ionic liquid used to dissolve and blend the cellulose and the silk is 1-Allyl-3-methylimidazolium chloride (AMIMCl). This ionic liquid has shown strong dissolution capabilities in other studies for dissolving cellulose or silk samples [30, 42]. It also has been proven that AMIMCl can greatly help the silk protein maintain its original molecular weight [41]. This experiment's aim is to characterize the morphological and physical properties of regenerated blended film as a function of cellulose/silk ratio. Our results revealed significant and decisive influence of hydrogen bonds upon the formation of microfibril and β-sheets in the cellulose-silk films. This information can guide future

applications, for the structural attributes of the polysaccharide and proteins comprising the biomaterial dictate the material properties of the products.

2.2 Materials and Methods

Chemicals

Cellulose: Avicel microcrystalline cellulose (Techware: Z26578-0) was acquired from Analtech. Before use, cellulose powder was placed in a vacuum oven (30 inHg) at a temperature of 70 ^{o}C for 24 hours to ensure removal of water [48].

Silk: Cocoons of *Bombyx mori* mulberry silks were obtained from China. In order to remove the sericin coated on the silk fibers, silkworm cocoons were boiled in a 0.02 M $NaHCO_3$ (Sigma-Aldrich, USA) solution for 15 minutes, and then rinsed thoroughly with deionized water three times to remove sericin completely. The degummed silks were air dried overnight, and put into a vacuum oven (30 inHg) at room temperature to remove the moisture on their surface.

Ionic Liquid: 1-Allyl-3-methylimidazolium chloride ionic liquid was purchased from Alfa Aesar and was also pretreated before being used. The ionic liquid before use was placed in a vacuum oven (30 inHg) at 70 ^{o}C for 24 hours [48], to ensure that the water molecules were removed from the solvent.

Dissolution of Polysaccharides and Protein:

The pretreated AMIMCl is prepared to begin the dissolution process of the two biopolymers, microcrystalline cellulose and the Mori silk fibroin. In order to create the composite films, the silk and cellulose composition were set to 10% of the total solution weight. The AMIMCl will be the remaining 90% of the total weight. The AMIMCl was placed in a vial on a stirred hot plate at a temperature of 85 ^{o}C. The selected amount of Mori Silk was added to the solution of the ionic liquids. Upon silk dissolution, microcrystalline cellulose powder was added slowly. Upon the dissolution of both materials, the new blended solution was coagulated with water to regenerate a new film. The ratios were made based on cellulose/silk content by weight; (cellulose:silk) 10%:90%, 30%:70%, 50%:50%, 60%:40%, 75%:25%, and 90%:10%.

Preparation of Regenerated Blended Film:

The new blended solution was transferred between two glass slides. The slides were kept above 50 °C for 5 minutes to ensure that the solution was still in liquid state, guaranteeing film uniformity and an even spreading of the ionic solution. The slides were then placed in a cross pattern to ensure a constant shape of the film across trials. Then, the slides were transferred to a Teflon evaporating plate, where water was added to it. The water filled the plate until the slides were completely submerged in the water. The immersion in water provided the removal of the AMIMCl from the films. For three ten (10) minute intervals, the slides were removed from the water for 2-minutes at a time. After the last time interval, the slides were removed from the films, and the films were placed in a vacuum desiccator for 24 hours.

Characterization

Fourier transform infrared spectroscopy

Fourier transform infrared spectroscopy **(**FTIR) analysis was performed using a ALPHA-Platinum ATR-FTIR Spectrometer with Platinum-Diamond sample module from Bruker. Data was collected at spectra range from 4000 cm^{-1} to 400 cm^{-1}; with 128 background scans and 32 sample scans at a resolution of 4 cm^{-1}. The average spectrum was collected from 6 different locations in the film. The FTIR diamond and hammer were cleaned between every sample with acetone.

Scanning Electron Microscope

The images for scanning electron microscopy were taken using the LEO1450EP SEM from Zeiss. The magnification of all images is 2000x, the scale is 10μm, and filament type is W (Agar A054). The SEM images are used to find the topography and the composition of the films. To prepare the films for SEM imaging, each sample was cut into rectangular pieces with a length between 5-10 mm. The samples were then placed into a Denton Desk II Au-Pd sputter coater. The system was pumped and stabilized to 75 millitorr. After the vacuum was stabilized, the samples were coated for 60 seconds. This added a layer of Au-Pd coating that was ~200Å thick. Once coated, the samples were ready for SEM imaging.

Thermogravimetric Analysis

Thermal gravimetric analysis (TGA) was performed using on average 6 mg samples on the TA Instruments Discovery system; all samples were in a nitrogen atmosphere. Samples were heated linearly with a 10 ^{o}C/min ramp up to 650 ^{o}C. Step transition analyses were performed for each sample to determine the onset of decomposition ($T_{95\%}$) and the weight-loss percentage of the sample evolved during the main decomposition step. Derivative values were calculated and peak height analyses performed to determine the temperature at which the samples decomposed at the highest rates ($T_{\Delta Max}$).

Differential Scanning Calorimetry

The film samples (each about 7 mg) were encapsulated in Al pans and heated in a TA Instruments (New Castle, DE) Q100 DSC, with purged dry nitrogen gas flow (50 mL/min), and equipped with a refrigerated cooling system. The instrument was calibrated with indium for heat flow and temperature. Standard mode DSC measurements were performed at a heating rate of 2 K/min from −30 to 320 °C.

X-ray Scattering

X-ray scattering was performed with the multi-angle X-ray scattering system (MAXS) at the University of Pennsylvania. The MAXS system uses Cu-K alpha X-ray radiation with l=0.154 nm from a Bruker Microstar generator operated at 45 kV and 60 mA. The bright, highly collimated beam was obtained via Osmic Max-Flux optics and pinhole collimation in an integral vacuum system. The scattering data were collected using a Bruker Hi Star two-dimensional detector with sample-to-detector distances of 11, 54, and 150 cm. The intensity reported is not absolute intensity and, thus, is reported in arbitrary units (a.u.). All samples were dried in vacuum for 24 hours before X-ray scattering characterization. As-received samples were dried, cut and inserted into 1 mm glass capillary. The X-ray scattering profiles were evaluated using Datasqueeze software; first, the isotropic 2-D scattering patterns were azimuthally integrated to yield intensity versus scattering angle. The background was subtracted from an empty 1 mm glass capillary. The crystal size was calculated using the Scherrer's equation from the (200) peak width for the

crystalline and semicrystalline blended films [49]. For a normal wide-angle X-ray scattering region in the 5 to 25° 2θ range for crystalline and semicrystalline films, see Supplemental Information.

2.3 Results/ Discussion:

Qualitative data made from observations showed that the majority of the films were physically firm and solid as silk concentration increased from 10% to 50% by weight. Samples above 50% lost some of their mechanical stability resulting in glassy material. At 90% silk film (10% cellulose), the film stability was very low as the material could easily fracture and break. These visible changes could provide evidence of a disruption in the cellulose and protein crystalline domains, causing structural stability changes as a function of material content [11, 50, 51]. The various characterization techniques presented below provide additional information that partially explains these qualitative results.

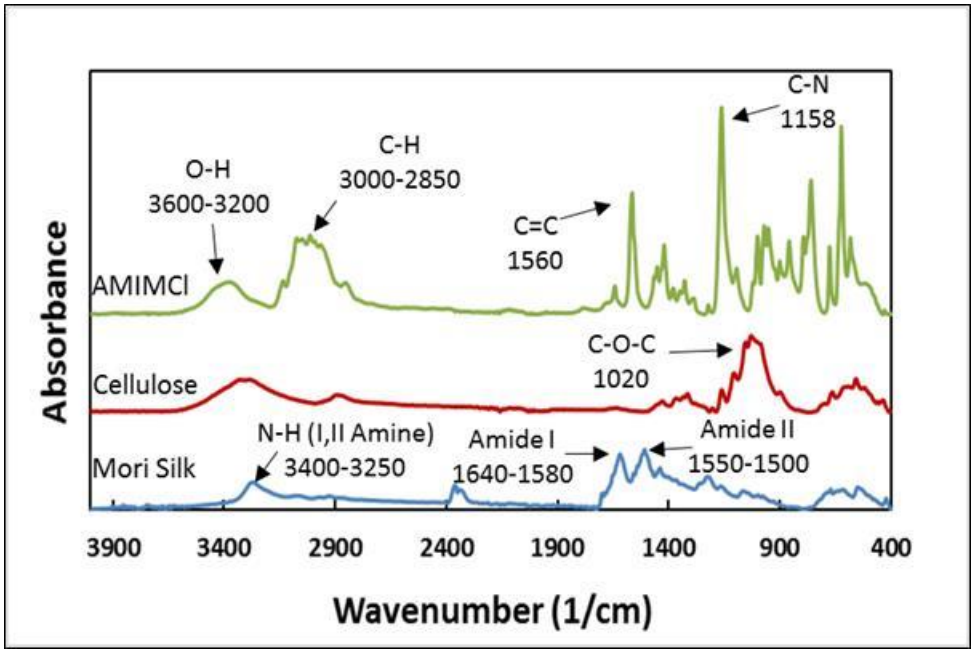

Figure 2.1. *Individual FTIR spectra for pure samples and ionic liquid. The three main components are shown with their key respective absorption bands.*

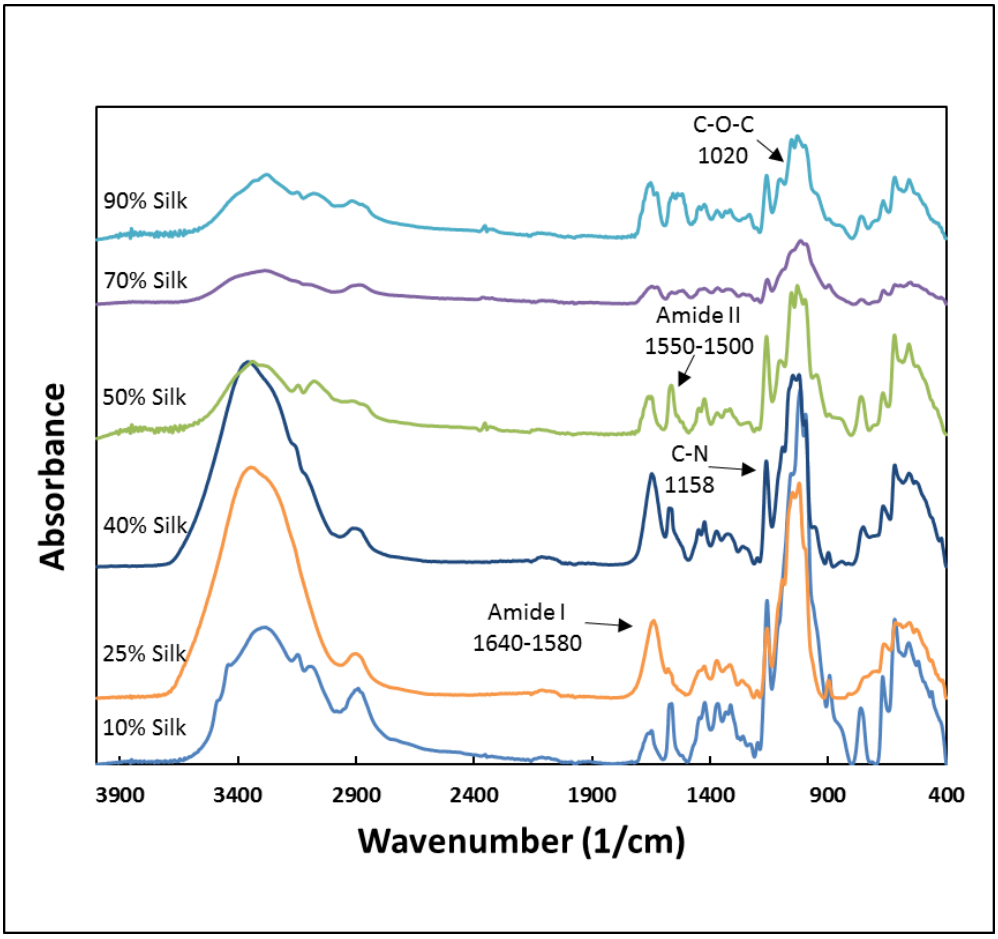

***Figure 2.2**. Stacked IR spectra of regenerated blended films. The spectra show absorption locations and shifts that occur in the film. The data can be compared to Figure 2.1 to show the interactions that are occurring in the film.*

Figure 2.1 shows the FTIR data for the pure ionic liquid, silk and the microcrystalline cellulose. The films exhibit peaks in the 3600-3200 cm^{-1} region, representing O-H bonds characteristic of cellulose. Additionally, the amine peak (N-H) is seen at 3400-3250 cm^{-1} and is characteristic of the silk. The alkene peaks exhibited at 3000-2850 cm^{-1} are also observed from the AMIMCl. The silk contains Amide I and Amide II peaks at 1640-1580 cm^{-1} and 1550-1500 cm^{-1}, respectively. The absorption band at 1560 cm^{-1} is the imidazolium ring, which contains a carbon double bond inside the aromatic ring structure of the AMIMCl. Another notable AMIMCl peak observed is a component of the ionic liquid structure C-N bond located at 1158 cm^{-1}. The last major peak that is identified is that of the cellulose structure, located at 1020 cm^{-1} and corresponding to the C-O-C

bonds. Small absorbance peaks are seen at a slightly higher wavenumber corresponding to the common C-O-C functional groups in the pure substances.

Figure 2.2 shows the spectra for the regenerated films at various concentrations. The film samples collected share all the major peaks corresponding with those of the pure samples. For example, the O-H at 3600-3200 cm^{-1} and the amine peak at 3400-3250 cm^{-1} are present in all the samples. However, the amide I and II peaks are shifted slightly to a higher wavenumber as compared to the pure silk sample (**Figure 2.1**). This is repeated in all the blended films. This is most likely due to the differences in β-sheets structural integrity between blended and pure silk. In the pure silk, β-sheets remain intact and are not disrupted. In the blended material, though, the β-sheets are disrupted by the inter- and intra-molecular interaction that occur between the cellulose and silk, an observation detected by others [11]. Therefore, the shift in the amide groups can be accounted for by the β-sheets disorganization and disruption in blended cellulose/silk films [21]. It is critical to mention that, as the dissolution occurs, secondary structures are broken down, changing the conformation of the polymeric chains. Upon coagulation by water, regeneration occurs but the molecular conformation will be disrupted on the level of hydrogen bonds in the various blended materials. This causes the alteration of the β-sheet configuration.

The samples that contained a higher ratio of cellulose showed C-O-C peaks at 1020 cm^{-1}. A pattern is observed from high to low concentration of silk, increasing carbon-nitrogen (1560 cm^{-1}) and carbon-carbon double bonds (1158 cm^{-1}) peaks that represent the aromatic ring of AMIMCl. This demonstrates that there may be a small presence of ionic liquid remaining in the sample. These C-O-C peaks and AMIMCl peaks suggests that the mixture is holding together.

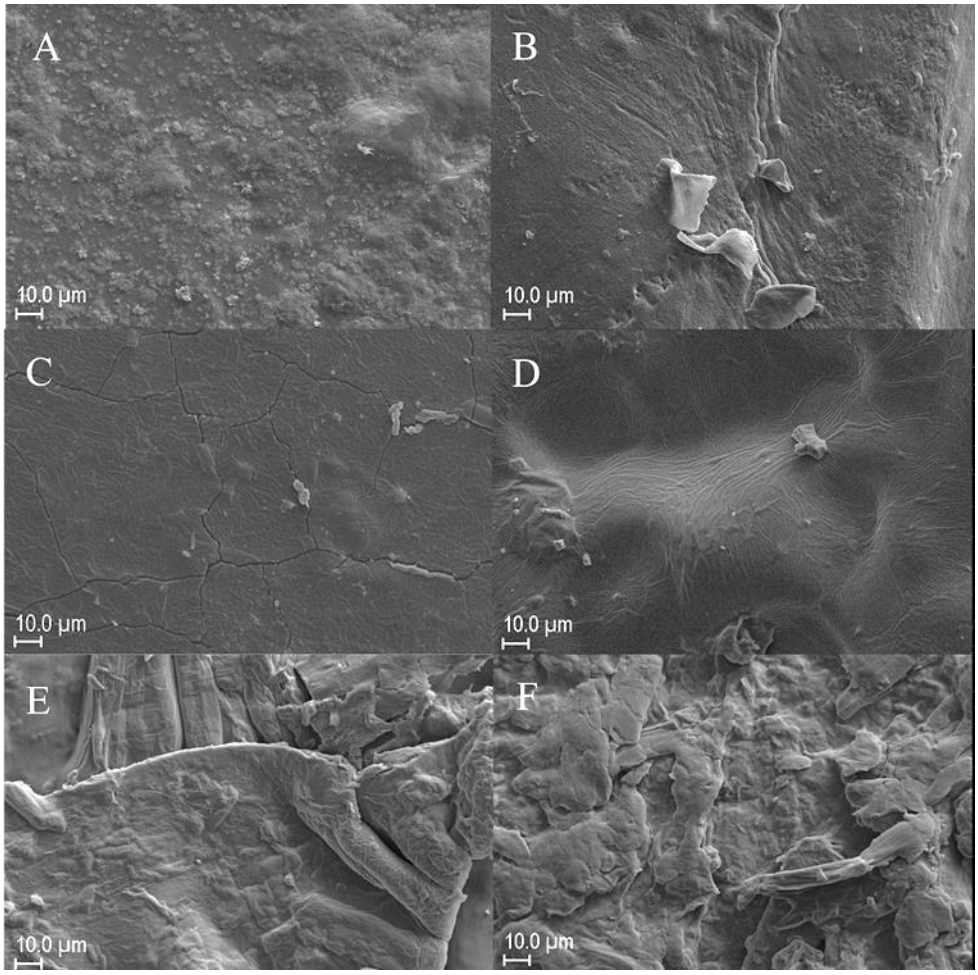

***Figure 2.3**. SEM images for (A) 10% silk, (B) 25% silk, (C) 40% silk, (D) 50% silk, (E) 70% silk, and (F) 90% silk.*

The SEM images provide insight into the surface structure of the materials, as shown in **Figure 2.3**. Observed from the lowest concentration of silk, it is noted that there are grainy/spherical structures at the surface (Figure 2.3A). When comparing Figures 2.3B to 2.3C, the surface of the film for 40% silk is more unified and smooth. As the concentration of silk increases, for the samples with 40% silk and 50% silk, a fibrous pattern begins to form. Profound fibrous patterns are observed when Mori silk and cellulose are blended in equal ratios, as observed in Figure 2.3D. This suggests that strong intermolecular interactions occur between the Mori silk and cellulose at this concentration. Interestingly, as the silk becomes the majority of the film's composite ratio, a significant change is noticed. The structure transforms from a grainy/spherical or smooth texture, at

lower concentrations, into a rough morphology with no noticeable patterns, as observed in the structure of Figure 2.3E, with 70% silk concentration by weight. The structure that is formed appears to be a disorganized/string-like formation. As the silk ratio continues to increase, as seen in the 90% silk concentration (Figure 2.3F), the formless structure of the film becomes more apparent. The high concentration of silk does not exhibit any defined characteristics seen in the prior samples. This observation was also originally detected in our qualitative observation analysis of the regenerated film.

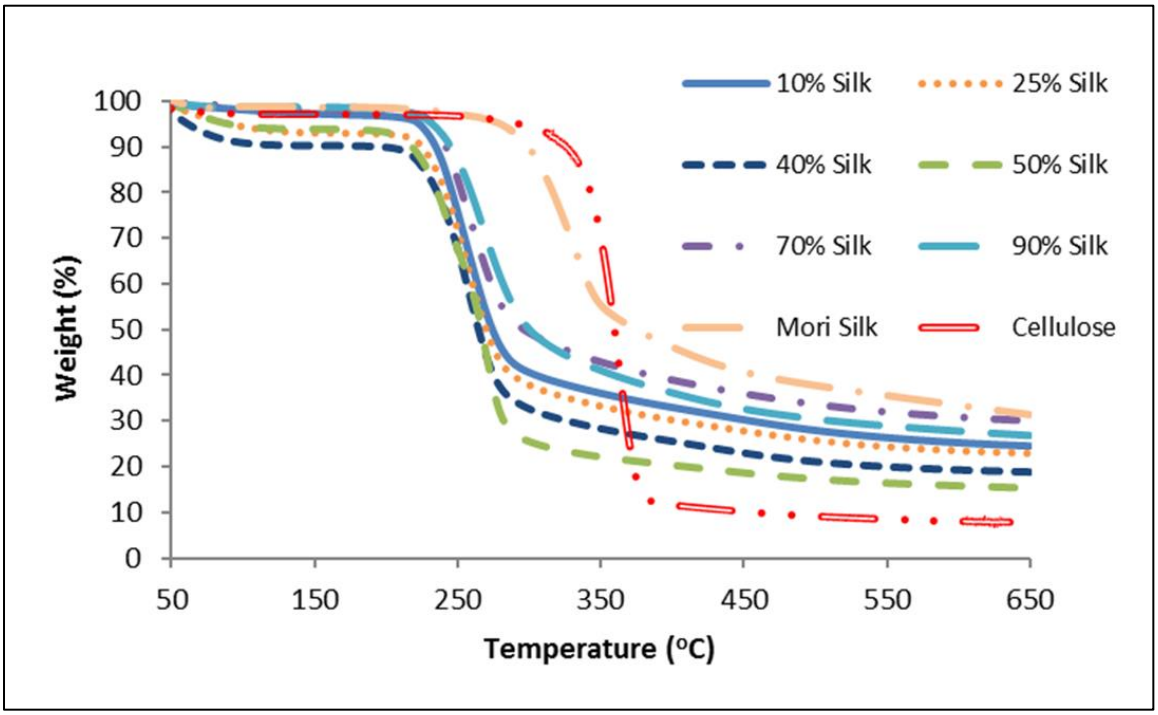

Figure 2.4. *Thermal gravimetric thermograms for the blended films and pure samples. Trends and decomposition temperature data are shown in Table 2.1.*

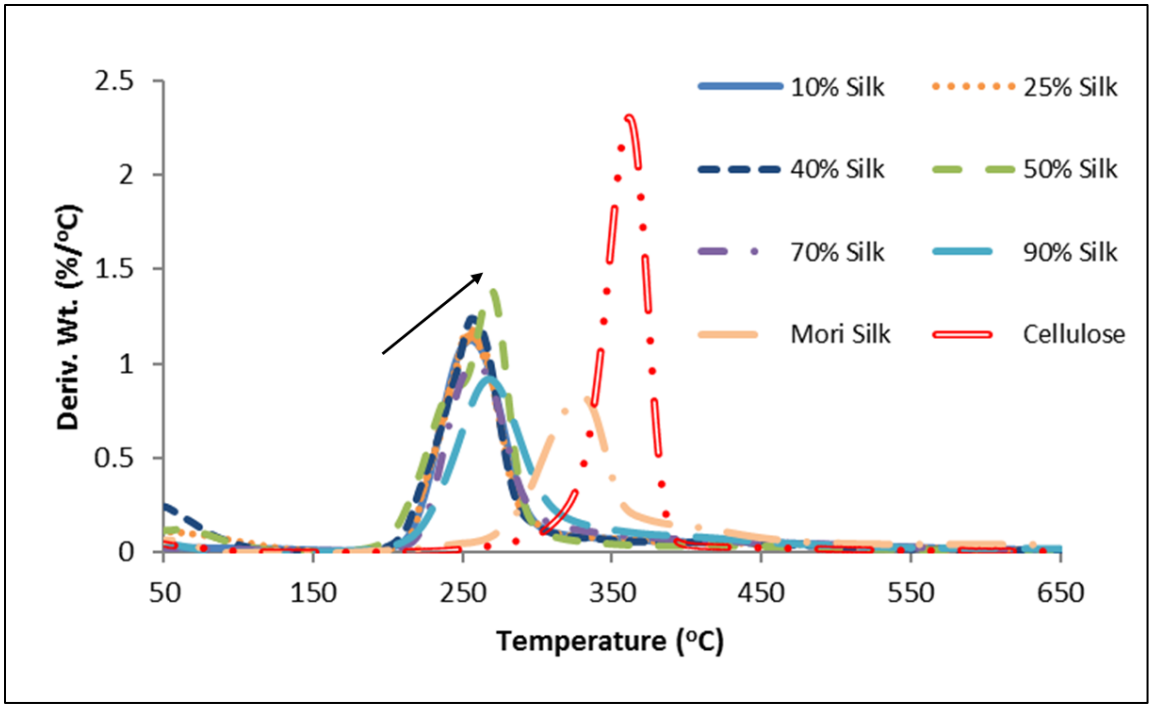

Figure 2.5. *Derivative % weight loss thermograms comparing the highest temperature peaks where most of the thermal decomposition of the blended materials occurred. Arrow shows increase in decomposition temperature as silk content increases.*

Table 2.1. *The starting and ending temperature of decomposition for various materials, along with the derivative value that gives the temperature when maximum decomposition occurs. Note that 50% silk has two values, in this case there are two peaks seen in the derivative plot.*

Sample	T_{Onset} (°C)	T_{End} (°C)	Wt. Loss (%)	$T_{\Delta Max}$ (°C)
Crystalline Cellulose	341.2	374.7	86.9	361.4
Mori Silk	294.9	357.9	60.9	329.9
10% Silk	231.8	283.3	69.3	255.5
25% Silk	231.8	282.6	67.3	256.6
40% Silk	232.4	281.4	69.24	258.2
50% Silk	239.4	283.7	76.7	245.4* 268.8*
70% Silk	235.5	289.3	64.7	258.3
90% Silk	240.4	303.5	68.4	267.8

Figure 2.4 shows the thermograms for the pure samples without ionic liquid and blended films. To initiate our analysis, it is noted that the pure samples, silk and microcrystalline cellulose, are more stable than the blended films. This is expected since the microcrystalline cellulose has crystalline domains and the silk fiber has β-sheet crystal formations. In addition, the pure samples do not retain water as compared to the blended films as shown between the temperature ranges 50 to 110 °C. This region is related to the small elimination of water molecules in the samples due to the hydrophilic properties of the blended materials. For example, the water retention and elimination of water is higher

for 50% silk than 10% silk because the sample with 50% silk is amorphous while the 10% silk is semicrystalline. This will be apparent in the X-ray scattering section. **Table 2.1** shows that pure silk and cellulose exhibit higher degradation temperature at 294.9 and 341.2 °C, respectively. For the blended materials, the weight loss percentages for all samples are similar, with up to 5% difference between each film sample, with the exception for the 50% silk that has a higher weight loss. It is worth indicating that the temperature of decomposition varies as the ratio of silk increases indicating possible morphological alteration. For example, for the lowest concentration of silk at 10% the temperature of maximum decomposition is at 255.5 °C. Alternatively, for 90% silk, the maximum decomposition is at 267.8 °C, indicating an increase in thermal stability.

The 50% ratio is the most thermally stable of all the blended film combinations, as seen in **Table 2.1** and **Figure 2.5**. Because of the homogeneous structures, the blended materials show similar TGA data, and the system error can account for the acceptable subtle difference among the samples with lower silk content (50% and below). Unlike the other samples that are in the 60% weight loss range, the 50% ratio sample has a larger weight loss percentage, 76.7%. Comparing this data to the derivative graph, it is seen that the 50% silk has been split into two peaks and the values are presented in **Table 2.1**. The ratio is spaced to be perfectly half cellulose and half silk to account for this peak splitting. As also evidenced in **Figure 2.3**, 50% silk concentration has a more uniformed structure that is formed from the combination. At 70% silk sample, the maximum degradation temperature is 258.8 °C and finally at 90% silk ratio it increased to 267.8 °C. At 70% silk, the blended film is amorphous and at 90% silk the film is semicrystalline, which is also confirmed by SEM and X-ray scattering. This suggests that the thermal stability increases with increasing silk content. The evidence provided can be compared with a study using only Mori silk: as the concentration of the silk increases, the interactions among the fibroin chains increase. This means that as the silk content increases, the silk chains are able to interact with each other without difficulty [52].

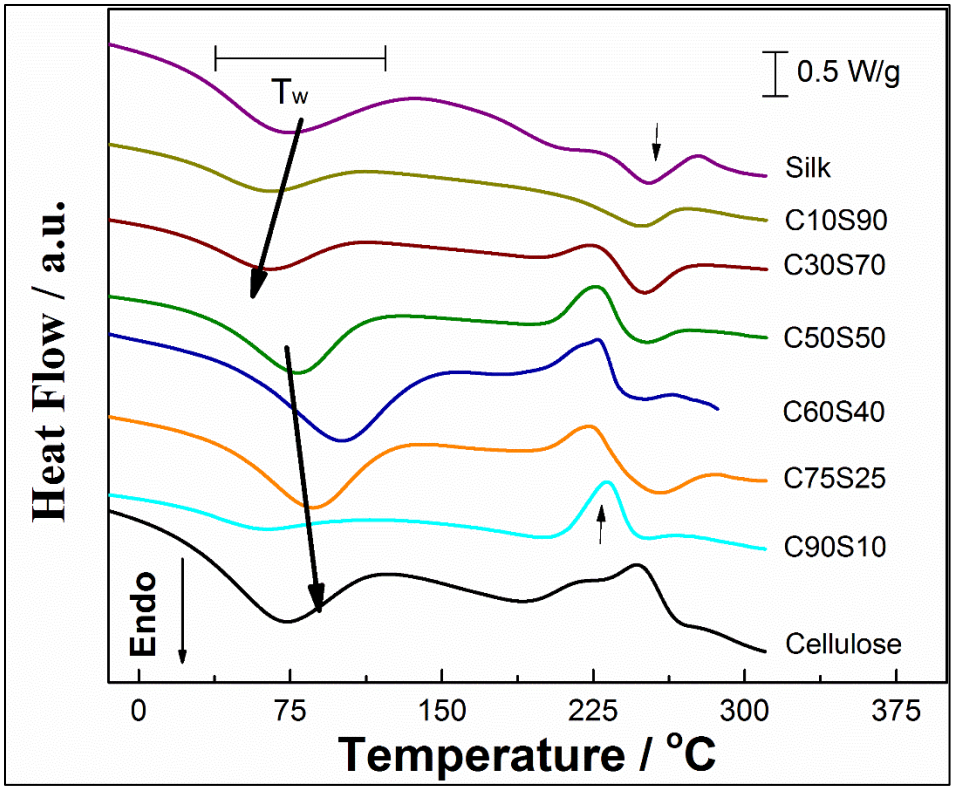

***Figure 2.6**. Standard DSC scans of the silk and cellulose composite films (From bottom to top, pure cellulose 10% silk, 25% silk, 40% silk, 50% silk, 70% silk, pure silk). The samples were heated at 2 °C/min from -30 to 320 °C.*

Continuing with additional data analysis, the standard DSC data presented in **Figure 2.6** further confirms blending. All of these samples show a blend-bound solvent transition peak centered between 70-100°C for water. It has been found that the glass transition of pure cellulose strictly depends on the bound water content in the films [53]. When bound water content is around 5%, the glass transition temperature of pure cellulose is 50-70°C [53]. Since our TGA results have demonstrated that there are always about 5-10% of bound solvent in the dried films, this transition peak could be due to a mixed glass transition of cellulose blend-bound solvent, as well as the evaporation of bound solvent just after the glass transition. Similar phenomena have also been found previously for the pure silk films with bound water molecules [20].With the increase of silk content, the first transition peak temperature first increases, but then decreases again when silk content is above 50%. The highest transition peak appears around 100 °C when the ratio of silk is

40%, indicating that the blended film tends to become the most stable around this mixing ratio. Our SEM and TGA results also confirmed this result. After the first transition, a strong non-isothermal crystallization peak appeared around 230 °C, and shifted from 246 °C (Cellulose) to 212 °C (C30S70), which is related to the thermal crystallization of the silk-cellulose blends. As the content of silk increases, the non-isothermal crystallization peak is diminishing. No separated individual crystallization peak for the cellulose or silk component were observed in the blends, which indicates that silk and cellulose were well blended to a homogeneous system without immiscibility. After crystallization, a degradation peak around 248 °C was shown for all silk containing samples. The pure cellulose, however, did not show a strong degradation peak along the baseline until 310 °C. As the concentration of the silk in the blend is greater, the degradation peak around 248 °C becomes sharper, which suggests the thermal degradation characteristics are mainly due to the silk component. The DSC information gathered here is of the utmost importance as it confirms the data observed in the TGA and SEM.

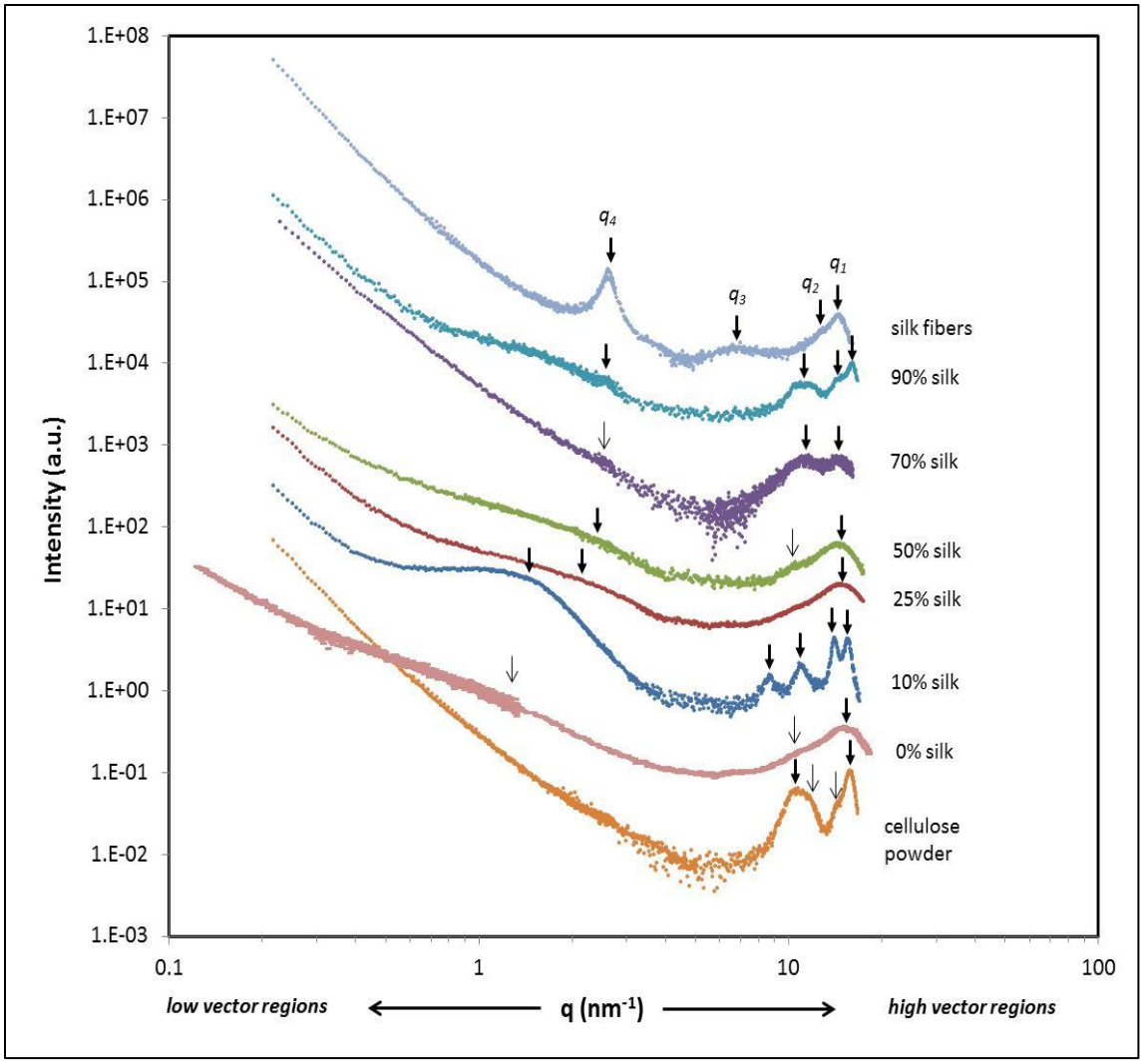

Figure 2.7*. X-ray scattering profiles of different silk-cellulose blended films. The intensity is offset to be able to distinguish between the various scatterings. The arrows indicate the location of each scattering peak.*

X-ray scattering was then used to probe the morphology of the pure materials and the regenerated films (comprised of varying silk content) over a wide range of scattering angles (wide angle, intermediate angle and small angle). **Figure 2.7** shows the scattering profiles of each sample recorded at room temperature. For a normal wide-angle X-ray scattering region in the 5 to 25°, 2θ range for crystalline and semicrystalline films, see **Supplemental Information**. We initiated our morphological investigation by looking at distinct spacing observed in the pure materials (*e.g.* silk fiber and cellulose powder) and regenerated 100% cellulose film.

For the silk fibers, we observed four scattering peaks moving from high to low scattering vector regions. The peaks are located at q_1=14.50 nm^{-1}, q_2=12.65 nm^{-1}, q_3=6.60 nm^{-1}, and q_4=2.62 nm^{-1}. The *d*-spacing for each peak is calculated by using the $d=2\pi/q$ formula, are d_1=0.43 nm, d_2=0.50 nm, d_3=0.95 nm, and d_4=2.40 nm, respectively. The *d*-spacing observed at 0.43 nm corresponds to the distance between β-strand, the distance at 0.50 nm corresponds to the distance between β-strand oriented perpendicular to the fiber, the distance at 0.95 nm corresponds to the inter-sheet distance between β-sheets, and the distance at 2.40 nm corresponds to the size of the β-sheets in the lateral direction [54-60]. In cellulose powder, two distinct spacings are observed. The spacings in cellulose can be attributed to its monoclinic unit cell of cellulose I_β equatorial lattice planes (q_1=15.75 nm^{-1} and q_2=10.61 nm^{-1}). Between q_1 and q_2, there are two small peaks at q_a=14.22 nm^{-1}, and q_b= 11.9 nm^{-1}. The calculated *d*-spacings are d_1= 0.40 nm, d_2= 0.60 nm, d_a= 0.44 nm, and d_b= 0.53 nm. In support of our data, Vainio reported crystalline monoclinic cellulose of Avicel with a scattering vector and reflection values of 15.7 nm^{-1} (200), 11.84 nm^{-1} (110), and 10.5 nm^{-1} ($1\bar{1}0$) [61]. Similar results were reported by Helbert, where he showed a high resolution image of the cross-sectioned *Halocynthia papillosa* microcrystal [10]. The 0.6 nm index is related to the longer side of the square structure which is always parallel to a side of the crystal. Herbert *et al* suggests that the cellulose microfibrils could be the packing of several sheets of the 0.6-nm lattices. The crystal size estimation for the Avicel using the Scherrer equation is 3.97 nm, which matched the published data of related systems [62-66].

The regenerated 100% cellulose film (0% silk) was made from microcrystalline cellulose (Avicel) and ionic liquid, coagulated with water and dried as stated in the experimental section. This particular sample was prepared as part of a previous study and its complete data analysis is presented elsewhere [67]; it is shown here for comparison purposes only. The typical sharp crystallization reflections which are characteristic of pure microcrystalline cellulose are not observed. Instead, the regenerated 100% cellulose film shows a broad peak at q_1= 14.57 nm^{-1} (d= 0.43 nm) that is indicative of an amorphous polymer. This is a typical transformation of cellulose I crystalline to amorphous cellulose structure [33]. This distance is related to the regenerated cellulose polymer backbone to backbone spacing. The interaction between the polymer molecule and the ionic liquid

changes the conformation of the cellulose polymer and upon coagulation with water, the crystalline domains cannot be formed. It is known that the transformation of cellulose upon coagulation is dominated by temperature, coagulator, coagulation time and ionic liquid electronegativity [32]. Upon further inspection into the 100% regenerated cellulose scattering profile, two small peaks (shoulders) can be observed: one is located between the intermediate and low scattering vector profile at q_a= 10.61 nm^{-1} (d_a= 0.59 nm) and the other is located in the low scattering vector region between 0.33 to 3.10 nm^{-1} (17.0 to 2.41 nm). For the latter, the maximum height of the peak is located at q_b=1.28 nm^{-1} (d_b= 4.91 nm). This region is related to the average microfibril cross-sectional dimension. Ibbett *et al.* has reported that microfibril cross-sectional dimension for eucalyptus pulp has a value of 3.6 nm [68]. In another study, Ioelovich *et al*. reported a value of 4.0 to 4.5 nm for corn cobs [69]. The diameter of microfibrils are known to range from about 2 to 20 nm [70]. The morphological information gathered from these three materials is critical to begin our understanding of the blended films.

The scattering profile for 10% silk blended film showed five characteristic spacings: q_1= 15.72 nm^{-1}, q_2= 14.20 nm^{-1}, q_3= 10.9 nm^{-1}, q_4= 8.70 nm^{-1}, and q_5= 1.50 nm^{-1}. The *d*-spacing for each peak is d_1 = 0.40 nm, d_2 = 0.44 nm, d_3 = 0.58 nm, d_4 = 0.72 nm, and d_5 = 4.19 nm, respectively. The sharpness of the various peaks at higher scattering vector is indicative of a semicrystalline nature of the blended material. The scattering spacing confirms the presence of the various macromolecules in the new regenerated biopolymer. It clearly shows the crystalline regions related to cellulose (q_1= 15.72 nm^{-1} and q_3= 10.9 nm^{-1}) as compared to the cellulose powder, as shown above, and the scattering vector peaks related to silk fibers (q_2= 14.20 nm^{-1} and q_4= 8.70 nm^{-1}), all as compared to the pure components. One can notice that the locations of these scattering peaks are very similar to the pure components with the exception of q_4. In general, cellulose I, upon coagulation, would disassemble to cellulose II or amorphous cellulose in ionic liquids; however, recrystallization back to an intermediate structure resembling cellulose I is observed at this low silk content. Recrystallization back to cellulose I has been reported at temperatures of 50^{o}C and under various experimental conditions [32, 33]. Furthermore, it has been reported that constraints or crystallization disruptions due to larger molecules or as a function of the type of ionic liquids could have a direct effect on the recrystallization

of cellulose intermediate structures [32-34, 71]. This was also observed on silk fibroin/cellulose blended films, where it was reported that an intermediate structure formed upon blending [34].

In our results, a small percentage of silk with cellulose causes a type of disruption for the cellulose to recrystallize to an intermediate structure resembling cellulose I, as shown in **Figure 2.8**. In this case, the X-ray scattering data indicates that some of the cellulose units are preserved. From the X-ray scattering *d*-spacing calculation for the 10.5 nm^{-1} ($1\bar{1}0$), we notice that the spacing decreases from 0.60 to 0.58 nm. This could indicate possible changes to the intra-molecular interactions. The scattering peak q_4 at 8.70 nm^{-1} corresponds to the inter-sheet distance. However, in this case it is not the inter sheet distance between β-sheets, in this case it is the inter sheet distance between a β-sheet and a cellulose sheet. The distance is reduced by 25% as compared to pure silk, which is about the average distance between the inter sheet distances of β-sheet in pure silk (0.95 nm) and the cellulose powder sheet (0.60 nm). These results confirm that the cellulose molecules are indeed interacting with the silk molecules. Moreover, the scattering peak at 1.50 nm^{-1} (4.19 nm) provides further evidence of this type of interaction between both cellulose and silk. This scattering peak corresponds to the interaction between the cellulose microfibril and the β-sheets of silk. The broadness of this peak suggests that the silk molecules are interacting with cellulose molecules at the microfibril region via hydrogen bonds. However, the lack of a clear periodicity prevents us from confirming very specific conformation. Interestingly, the crystallite size based on the Scherrer equation for this sample is 5.52 nm. The crystallite size is bigger than the one calculated for Avicel, thus we can conclude that other contributions (*e.g.* silk) are affecting the crystallite size. Each microfibril contains a single crystalline core, the same order size as the microfibril [62]. Earlier, we mentioned that the microfibrils consist of the packing of several cellulose sheets exhibited 0.6-nm spacing. In this case, it is a combination of the packing of cellulose sheet and cellulose/silk β-sheets that form the microfibril. It is imperative to recall that DSC data confirmed that all samples were homogenous. This agrees with the general knowledge that cellulose microfibril size can change due to interaction with other molecules. For example, there are strong interactions between cellulose and xylan in nature, and the amount of xylan

is known to affect the crystalline structure of cellulose and the size of the microfibrils [67, 72-74].

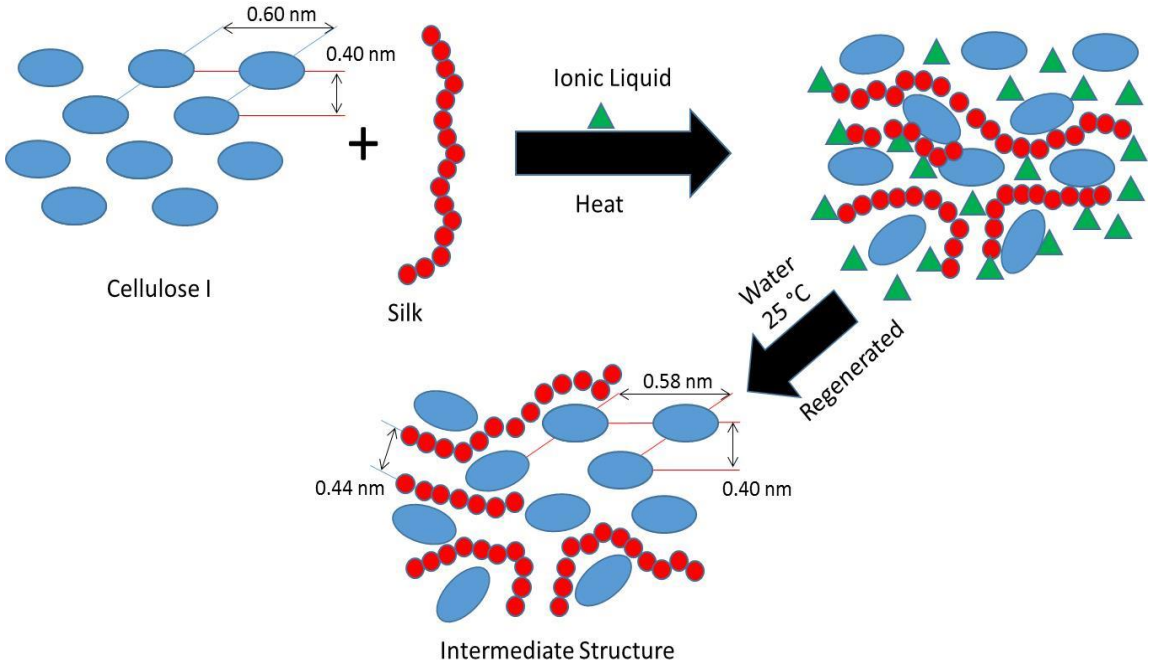

***Figure 2.8**. Schematic representation of the intermediate structure formation for the 10% silk blended film.*

In continuation with the blended films, we can detect that as the percent silk increases from 10% to 25% and 50%, the X-ray scattering profile shows one broad peak at high scattering vector region indicative of an amorphous morphology of the blended films. Herein, the cellulose changed from cellulose I to an amorphous structure. For both 25% and 50% silk, we observe a similar scattering vector at 14.90 nm^{-1}. The Gaussian curve is broad with a *d*-spacing of 0.42 nm and is interestingly in between the correlation distance observed from silk fibers and regenerated cellulose (0% silk). This distance is related to a combination of backbone to backbone distances between similar chains and the backbone to backbone spacing between different chains (silk and cellulose). At low scattering vector, we can observe the location of the scattering vector peak increases from 2.14 nm^{-1} to 2.38 nm^{-1} for 25% and 50% silk, respectively. We can notice that this scattering peak broadens gradually as compared from 10% to 50% silk. As previously discussed, this region is related to interaction between the cellulose microfibril and the silk β-sheets. These are

reasonable results as both 25% and 50% silk did not show semicrystalline regions nor inter sheet distance between β-sheets or cellulose sheets. Therefore, the conformation for both samples will be somewhat uniform. This can be confirmed in the SEM **Figure 2.3** where the topology for both 25% and 50% silk samples were similar. We also observed a thermal effect at 50% indicating possible changes in the morphology as compared to 10% silk.

As the silk concentration further increases from 50% to 70%, a transitional inter- and intra- morphological disorder between the blended materials can be observed. At 70% silk there are two scattering peaks at the high vector region: q_1= 14.5 nm^{-1}(d_1= 0.43 nm) and q_2= 11.44 nm^{-1} (d_1= 0.55 nm). The scattering profile data is noisy for this sample; however, we can still observe that the sample is not semicrystalline in nature (probably composed mainly of amorphous cellulose and silk). We suggest that the sample is in a transitional morphological stage, since the second scattering peak at q_2 is very broad. This region is indicative of the existence of an intercalation structure with the insertion of either silk into cellulose or cellulose into silk. This transitional stage also can be confirmed in the SEM images and the thermograms, as discussed previously (**Figure 2.3, 2.4 and 2.6)**. At low scattering vector, a small peak at 2.49 nm^{-1} with a *d*-spacing of 2.52 nm, is noticeable. This peak is related to the β-sheets lateral distance as demonstrated from the pure silk fibers profile. In this sample, minimal cellulose microfibril formation is observed due to the lack of cellulose crystalline structures.

Finally, in 90% silk we can also observe three additional scattering peaks at q_1= 15.80 nm^{-1}, q_2= 14.50 nm^{-1}, and q_3= 11.25 nm^{-1}. The *d*-spacings are d_1 = 0.40 nm, d_2 = 0.43 nm, and d_3 = 0.56 nm. For this sample, the scattering peaks at the high vector region are very sharp, indicating that the cellulose component has recrystallized to intermediate cellulose I structure and combined with silk molecules. The scattering peak at q_1= 15.80 nm^{-1} is related to cellulose and the scattering peak at q_2= 14.50 nm^{-1} is related to the silk, similar to the 10% silk film. We can observe the interaction between molecules alike (cellulose-cellulose and silk-silk) and the interaction between silk and cellulose. We can also observe that the spacings of the strand regions are affected by the interaction between different molecules as shown from the scattering peak at q_3= 11.25 nm^{-1}. One could think that the distance between strands increases due to the interaction with the monomers in the

cellulose structure, suggesting the formation of new crystalline sheets composed of silk:cellulose:silk. The scattering peak seems to be composed of two Gaussian peaks: one is related to the longer side of cellulose crystals, while the other is related to the distance between β-stands in silk. This could also suggest that the silk anchors into the cellulose backbone via hydrogen bonding, similarly to the interaction between cellulose and glycoproteins (connected with pectin) or the interaction between chitin and protein [75]. Additionally, we can notice this interaction again in the formation of microfibrils whereas, in this case, the β-sheets seem to dominate, as silk concentration is the highest. The scattering peak is located at 2.59 nm^{-1} (2.42 nm). The crystallite size for this sample calculated from the Scherrer equation is 2.10 nm, in the same range as the size calculated by X-ray scattering. It is smaller because there are more silk-to-silk interactions. It is interesting to note that the microfibril size decreases as the percent silk increases. For example, **Table 2.2** shows the low scattering vector peaks and their correlation distances for all blended films. As the data in the table demonstrates, the correlation distance decreases as the percent silk content increases, while reducing the cellulose content. This suggests a spatial reorganization that depends on the concentration of the blended material and its semicrystalline nature. At low silk content, the cellulose micro fibril size is disrupted by the protein molecules; however, its size and interaction is reduced as the silk content increases, causing the film to be either amorphous or semicrystalline. We also observed similar changes as a function of silk in the FTIR.

In summary, the X-ray scattering profiles for 10% and 90% silk showed semicrystalline structure while the X-ray scattering profiles for 25%, 50% and 70% silk samples showed amorphous structures. The transformation from cellulose I to cellulose II was not observed for 10% and 90% silk samples. Instead, a modified or intermediate crystalline structure was composed resembling that of cellulose I and silk. We can also confirm that as the silk content increases, the level of disruption in the β-sheets formation reduces while also disrupting the microfibril integrity resulting in an increase in thermal stability. One possible interpretation is that the semicrystalline nature of the blended film, at 10% and 90% silk, reorders with the amino acids stacked chains of silk in a face to face manner. The crystallite sizes for the semicrystalline films based on the Scherrer calculation are in the same range as the one estimated from the X-ray scattering. The various results

enable us to conclude that inter and intra- molecular interactions between the silk and cellulose molecules control the thermal and morphological properties of the blended materials. Future computer simulations could provide a clear view of such morphological findings.

Table 2.2*. The lower scattering vector peaks and corresponding d-spacing for each blended film. It is noted that as the silk content increases, the d-spacing decreases up to a point where the β-sheet formation dominates, as in pure silk.*

Sample	Scattering Vector (nm^{-1})	d-spacing (nm)
Cellulose Powder	N/A	N/A
0% Silk	1.28	4.90
10% Silk	1.50	4.19
25% Silk	2.14	2.93
50% Silk	2.38	2.64
70% Silk	2.49	2.52
90% Silk	2.59	2.42
Silk Fiber	2.62	2.40

2.4 Conclusion

These results provide evidence that the biomaterials films were successfully regenerated from a blending of cellulose and silk using 1-Allyl-3-methylimidazolium chloride as a solvent and water as the coagulator agent. The films exhibited similar characteristics according to their proportions of cellulose and silk. A reduction in hydrogen bonding was observed at higher silk contents. Various topological differences were observed as a function of silk content. Samples with 25% to 50% silk formed uniform patterns, while samples greater than 50% silk formed disorganized patterns. The DSC

confirmed that the samples were of a homogenous blend, giving evidence that the thermal degradation characteristics are mainly due to the silk component. The X-ray scattering confirms the various morphological variations as a function of silk content. The blended films formed intermediate semicrystalline or amorphous structures depending on the silk content. The cellulose microfibril diameter was altered by the addition of silk. In addition, the silk β-sheet dimension changed due to the inter- and intra-molecular interaction with the glucose units in the cellulose structure. Possibly, this alteration is a result of a developmental change in the cellulose microfibril during regeneration, with the cellulose/silk concentration dictating the way in which the β-sheets interact with the microfibril. The stability of the film's molecular structures varies according to the cellulose/silk ratio, thus impacting the thermal and structural properties. These results give important insight into the possibility of preparing tunable biomaterials, for the cellulose/silk proportions can be adjusted to optimize the desired properties by tuning the level of crystallization in the film. In future studies, this information can guide further projects intending to measure the impact of other ionic liquids and coagulating agents on the morphological features of biomaterials; especially as a function of temperature.

CHAPTER 3

Morphological and Thermal Properties of Silk/Cellulose-based Biomaterials as a Function of Ionic Liquid Type

3.1 Introduction:

Biomaterial research is continuing to be at a pivotal peak of interest in the community and research has led to new developments and discoveries in the medical, electrical and environmental sectors [2]. The medical community is interested in regenerative biomaterials that contain tunable properties, with minimally harmful human body interactions. This brings an interest in natural biomaterial products, as they have been used in recent studies due to their biocompatibility, tunable morphological and physical properties, along with being a low-cost material. Cellulose, a natural biomaterial, is one of the most abundant materials on Earth and it is found as cellulose I (α or β) form [10]. Cellulose is a polymer that has strong intramolecular and intermolecular hydrogen bonding [10, 13]. When cellulose I biomaterial is dissolved, and regenerated in solution, its crystalline structure changes from Cellulose I to either Cellulose II, amorphous or intermediate structure [32-34]. A disadvantage of cellulose biomaterials is that they are known to have a high stiffness and has very poor solubility in common solvents [12]. The material properties of cellulose can be tuned by blending the cellulose with other similar materials in solution. This will allow for an increase in intra- and inter-molecular interactions for an improvement in morphological thermal and mechanical properties.

Proteins are another natural biomaterial that can be blended with cellulose. For example, *Bombyx mori* silk, a silk protein used in the textile industry can be obtained from silkworms, consisting of several fibroin protein fibers and are coated with a layer of sericin. Mori silk fibroin fibers are made of thousands of parallel fibrils consisting of repetitive amino acid sequences of $(GAGAGS)_n$, which can form insoluble stacked β-sheets crystallized in the fiber. The Mori silk has many advantages that leads to its success in biomedical materials; biocompatibility, tunable degradation rate, abundance from natural or cultivation, stable structural and flexible properties [18]. When introduced and

regenerated the Mori silk materials have a high content of β-sheets [22]. Studies have shown that proteins strongly interact with polysaccharides through hydrophobic-hydrophobic interactions and electrostatic interactions [22, 67, 76]. The polysaccharides are typically hydrophilic in nature and will control the aqueous phase rheology acting as a stabilizing agent of the protein-polysaccharide matrix [3, 22, 38, 39, 77]. Cellulose is important in blending the materials as it allows for the creation of new properties that will enhance the poor properties of the pure cellulose and protein sample, resulting in utilization in tissue and organ engineering and as implants in the medical industry.

The dissolution process is critical in making the blended material as the solvent controls the molecular interaction between the cellulose and silk. Poor solvents will affect the miscibility of the regenerated film causing a significant decrease in the mechanical properties [23]. Known issues that occur with the use of organic solvents are that they have adverse effects on proteins materials, by breaking the polymer chains thus destroying the molecular weight of the material [41]. Ionic liquids have been used to dissolve both cellulose and silk successfully without changing the molecular weight [25, 30]; however, an in-depth physico chemical and morphological study on the effect upon the biomaterial is still in short supply. Ionic liquids consist of a bulky, unsymmetrical ion containing a delocalized charge, allowing for a low melting point to occur [28, 43]. Ionic liquids can have a combination of properties unlike typical solvents such as, negligible volatility, reusability, non-flammability, high thermal stability, and high conductivity. They have an advantage over organic solvents as they do not lead to unwanted side products and are considered a green alternative as they encompass the ability to be reusable [43-46]. Studies on regenerated films in the past gave vague information on the driving force of the morphology changes as the miscibility is a critical step in the process to ensure that a homogenous blend can occur. It has been reported that anions are stronger hydrogen bond acceptors than cations [28, 78]. When biopolymers are dissolved in ionic liquids, the anion forms hydrogen bonds with the hydroxyl groups disrupting the naturally occurring hydrogen bonding network, and the cation associates with the ether oxygen atoms and CH group that occur in polysaccharides such as cellulose crystals [11, 28, 78]. The same reasoning also applies to dissolving proteins such as *Bombyx Mori* silk. However, to make use of this approach to generating useful biomaterials, we need to understand how the

anions or the cations affecting the inter- and intra- molecular interactions, morphology, and physicochemical properties of the regenerated biomaterial.

Thus, this study will investigate the structural, thermal, and morphology changes as a function of ionic liquid type, comparing similar cations with varying anions and vice-versa. The various ionic liquids allow for different interactions to occur based on the size and functional groups attached to the anion. This investigation will facilitate an understanding how the properties of the biomaterial can be modified by selected the appropriate type of solvent. The ionic liquids that are used in this study are; 1-Allyl-3-methylimidazolium chloride (AMIMCl),1-Butyl-3-methylimidazolium chloride (BMIMCl), 1-Ethyl-3-methylimidazolium chloride (EMIMCl), 1-Ethyl-3-methylimidazolium acetate (EMIMAc), 1-Butyl-3-methylimidazolium bromide (BMIMBr) and 1-Butyl-3-methylimidazolium methanesulfonate ($BMIMMeSO_3$). The major reason for using AMIMCl, EMIMCl, and BMIMCl, is that they have a similar structure with different alkyl chains, and allows for comparison to be made based on the hydrophobic effect upon the material properties. The other ionic liquids, EMIMAc, BMIMBr, and $BMIMMeSO_3$, have been less studied, leading to, perhaps, new information in regards to structure and morphology. The advantage of these three ionic liquids is that they contain a bulkier anion group which will increase the molecular interactions differently from those of the chloride anions. Some of the ionic liquids mentioned previously have been used in previous studies, in the investigations of the dissolution process of either silk or cellulose by various groups [59, 79-83]. The main focus of this study will be to explore the interactions between the type of ionic liquid and the selected biomaterial (10% silk and 90% cellulose) and to understand how the β-sheet formation can disrupt or interact with the backbone to backbone spacing between molecules (alike and/or different).

3.2 Experimental

Chemicals

Ionic Liquids: 1-Allyl-3-methylimidazolium chloride ionic liquid was purchased from Alfa Aesar, 1-Butyl-3-methylimidazolium chloride, 1-Butyl-3-methylimidazolium methane sulfonate, 1-Butyl-3-methylimidazolium bromide, 1-Ethyl-3-methylimidazolium chloride, and 1-Ethyl-3-methylimidazolium acetate were all purchased from Sigma-Aldrich. The ionic liquids were pretreated by being placed in vacuum oven (30 inHg) at 70 °C for 24 hours [48], to ensure that the water was removed from the solvent.

Cellulose: Avicel microcrystalline cellulose (Techware: Z26578-0) was acquired from Analtech. Before use, cellulose powder was placed in a vacuum oven (30 inHg) and at a temperature of 70 °C for 24 hours [48].

Silk: Cocoons of *Bombyx mori* mulberry silks were obtained from China. In order to remove the sericin coated on the silk fibers, silkworm cocoons were boiled in a 0.02 M $NaHCO_3$ (Sigma-Aldrich, USA) solution for 15 mins, and then rinsed thoroughly with deionized water three times to remove sericin completely. The degummed silks were air dried overnight, and put into a vacuum oven (30 inHg) at room temperature to remove the moisture on their surface.

Dissolution of Polysaccharides and Protein:

The pretreated ionic liquid is prepared to begin the dissolution process of the two polymer biomass materials, microcrystalline cellulose and the Mori silk fibroin. In order to create the composite films, the silk and cellulose composition was made at 10% of the total solution weight. The remaining 90% of the total weight was the ionic liquid used in the dissolution process. The total solid weight of the silk and cellulose was broken down in a 10% silk and 90% cellulose composition. The various individual ionic liquids were placed on a stirred hot plate at 100 °C ±6 °C. The ionic liquids were placed in an oil bath to ensure temperature was spread evenly during the dissolution process. The selected amount of Mori Silk was added to the solution of the ionic liquid. Upon silk dissolution, microcrystalline cellulose powder was added slowly. Upon the complete dissolution of

both materials, the new blended solution was coagulated with water to regenerate a new film.

Preparation of Regenerated Blended Film:

The new blended solution is transferred between two glass slides. The slides are kept above 50 °C to guarantee film uniformity and for 5 min to ensure that the solution is still in liquid state. Then, the slides are transferred to a Teflon evaporating plate, where water was added to it. The water was filled to fully submerge the glass slides that were used. The films are submerged in the water for 48 hours to remove as much of the ionic liquid and allow for the regeneration of the blended film. After the 48 hours, the slides are removed and the solid film is put into a vacuum desiccator for 24 hours.

Characterization

Fourier transform infrared spectroscopy

Fourier transform infrared spectroscopy **(**FTIR) analysis was performed using a Bruker's ALPHA-Platinum ATR-FTIR Spectrometer with Platinum-Diamond sample module. Data was collected at spectra range from 4000 cm^{-1} to 400 cm^{-1}; 128 background scans and 32 sample scans at a resolution of 4 cm^{-1}. The average spectrum was collected for 6 different locations in the film. The FTIR diamond and hammer were cleaned between every sample with acetone. Fourier self- deconvolution studied the amide I region (1595-1705). Deconvolution was performed by using the Lorentzian line shape, with a 25 cm^{-1} half-bandwidth and a noise reduction factor of 0.3. The lines were then fit using the Opus 7.2 program corresponding with various vibrational band assignments in the amide I region. Gaussian profiles were used to allow for the fitting results and nonlinear least squares method was used created to allow for make the curve as close to the deconvoluted spectra [84].

Scanning Electron Microscope

The scanning electron microscopy was performed on Jeol's JCM-6000 SEM. The magnification of the images was 500, with a scale of 50 μm. The images were used to find the topography of the regenerated films. The films were prepared before use by cutting the

film into rectangular pieces between 5 to 10 mm. The samples were then placed into a Denton Desk II Au-Pd sputter coater. The system was pumped and stabilized to 75 millitorr. After the vacuum was stabilized, the samples were coated for 60 seconds, thus adding a layer of ~200Å thick Au-Pd coating. Once coated, the samples were ready for SEM imaging.

Thermogravimetric analysis

Thermal gravimetric analysis (TGA) was performed using the TA Instruments Discovery system with on average 6 mg samples; all samples were in a nitrogen atmosphere. Samples were heated linearly with a 10ºC/min ramp up to 650ºC. Step transition analyses were performed for each sample to determine the onset of decomposition ($T_{95\%}$) and the weight-loss percentage of the sample evolved during the main decomposition step. Derivative values were calculated and peak height analyses performed to determine the temperature at which the samples decomposed at the highest rates ($T_{\Delta Max}$).

Differential Scanning Calorimetry

The samples (around 5 mg) were encapsulated in aluminum pan and measured by a TA Instruments Q100 DSC equipped with a refrigerated cooling system (RCS) under the purged dry nitrogen gas flow (50 mL min^{-1}). The instrument was calibrated with indium for heat flow and temperature. Standard mode DSC measurements were taken at a heating rate of 2 K min^{-1} from -20 °C (253 K) to 400 °C (673 K). Temperature-modulated differential scanning calorimetry was performed at a heating rate of 2 K min^{-1} with a modulation period of 60 s and temperature amplitude of 0.318 K from -20 °C (253 K) to 400 °C (673 K). Aluminum and sapphire reference standards were used for calibration of the heat capacity through a three-run method.

X-ray Scattering

X-ray scattering was performed with the multi-angle X-ray scattering system (MAXS) at the University of Pennsylvania. The MAXS system uses Cu-K alpha X-ray radiation with l=0.154 nm from a Bruker Microstar generator operated at 45 kV and 60

mA. The bright, highly collimated beam was obtained via Osmic Max-Flux optics and pinhole collimation in an integral vacuum system. The scattering data were collected using a Bruker Hi Star two-dimensional detector with sample-to-detector distances of 11, 54, and 150 cm. The intensity reported is not absolute intensity and, thus, is reported in arbitrary units (a.u.). All samples were dried in vacuum for 24 hours before X-ray scattering characterization. As-received samples were dried, they were cut and inserted into 1 mm glass capillary. The X-ray scattering profiles were evaluated using Datasqueeze software; first, the isotropic 2-D scattering patterns were azimuthally integrated to yield intensity versus scattering angle. The background was subtracted from an empty 1 mm glass capillary, but not corrected for sample density.

3.3 Results/ Discussion:

The qualitative data obtained through observations was relevant as it showed that by varying ionic liquids, with a constant biomaterial composition, the topological and materials mechanical properties changed. The blended films regenerated AMIMCl, EMIMCl, BMIMCl, and EMIMAc were firm while the ones regenerated with BMIMBr and $BMIMMeSO_3$ were soft. One possible interpretation is that physical changes can be attributed to a disruption of the cellulose semicrystalline structure and protein β-sheets [11, 51]. The following characterization analysis will allow for additional information to understand these qualitative results.

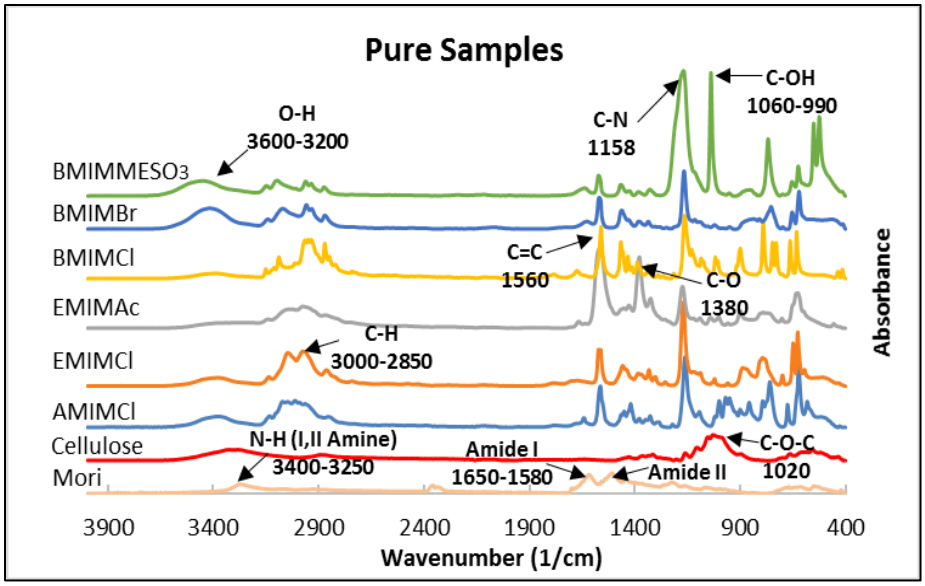

Figure 3.1. *Individual FTIR showing the key characterization bands located in the pure samples. The main components are shown with their respective absorption bands.*

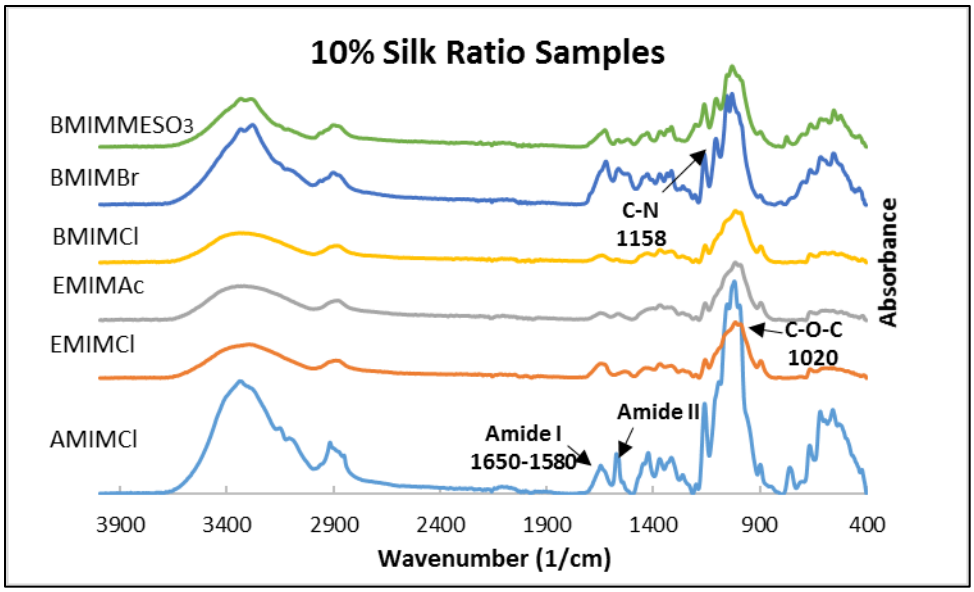

Figure 3.2 *Stacked FTIR spectra of the 10% silk-cellulose film samples showing absorption locations of the combined materials and the shifts that occur in the regenerated film. The data is comparable to that in Figure 3.1 by showing the difference in the regenerated film against that of the pure ionic liquids.*

Figure 3.1 shows the combined FT-IR data for the pure samples silk, cellulose, and ionic liquids. Common peaks exhibited can be observed in the 3600-3200 cm^{-1} region and are denoted by the O-H bond peaks that are found in the cellulose. The silk has a peak located in the 3400- 3250 cm^{-1} region corresponding with the amine peak (N-H). Moving into the alkane region at 3000-2850 cm^{-1}, the peaks vary depending upon the ionic liquid. The reason for this is due to the imidazolium cation functional group. Differences can be observed between the cation groups side groups seen in the BMIMCl which contain a butyl substituent and the EMIMCl with contains an ethyl substituent. The silk has two major peaks that are related to the Amide I and the Amide II peaks, which are located around 1640-1580 cm^{-1} and 1550-1500 cm^{-1} regions. Also, seen in this region is the imidazolium ring whose characteristic includes an aromatic ring containing a carbon double bond at 1560 cm^{-1}. At 1380 cm^{-1}, it is noted that there is a sharp peak for the EMIMAc, this peak corresponds with the C-O group. Another peak to observe is at 1158 cm^{-1}; this peak is a part of the C-N bond from the imidazolium ring. Finally, a peak worth noting is the cellulose absorbance peaks located around 1020 cm^{-1} corresponding to the C-O-C bonds of the cellulose.

Figure 3.2 shows the FT-IR for all blended films regenerated as a function of ionic liquid type. The similarities that are shown are the regions that contain the O-H at 3600-3200 cm^{-1} which are the same as the peaks of the pure samples observed in **Figure 3.1**. The peak at 3600-3200 cm^{-1}, related to O-H bond and at 3400-3250 cm^{-1}, related to the amine peak, is present in the all samples. The alkane regions are slightly different as they are less broad due to processing conditions; however, they still appear in the same location as those seen in the ionic liquids, silk, and cellulose. The peaks for Amide I and Amide II are shifted to a higher wavenumber, when compared to the pure silk sample. The shift is seen in all the regenerated film samples for each ionic liquid. The reasoning for this is due to the disruption of the β-sheets. As the pure silk exhibits non-disrupted β-sheets seen in **Figure 3.1**, which is the natural form. The regenerated films seen in **Figure 3.2** are disrupted on the inter- and intra-molecular level by the ionic liquid that was present in the system. This causes a difference in the interactions of the cellulose and silk that has been observed previously, accounting for the shift that is occurring with the β-sheets as there is now a disorganized β-sheet formation [11]. The shift is consistently seen in all the

regenerated film samples. This allows for the disruption to occur with the regenerated films for all ionic liquids [21]. This leads to the secondary structures being changed during the dissolution process. As the ionic liquid disrupts the hydrogen bonds, the overall shape of the β-sheet changes. Upon coagulation, a new conformation is formed. The conformational changes are important because this provides evidence that there is a way to control the formation of the regenerated film.

The carbon-nitrogen bond and carbon-carbon double bond found in the aromatic ring located in the ionic liquids can be observed at 1560 cm^{-1} and 1158 cm^{-1}. The absorbance of the peaks has been reduced in the regenerated films as compared to our previous publication [76]. This IR data confirms that most of the ionic liquid was removed. However, there are still traces of the ionic liquid seen in the film. When comparing the different blended films in **Figure 3.2**, small differences can be seen between the regenerated film samples. The most extreme changes are located with the $BMIMMeSO_3$ and the BMIMBr as they have simply greater molar absorptivity. This can be described as an interaction between the ionic liquid, silk, and cellulose components. The sharpness of the peaks of the $BMIMMeSO_3$ and the BMIMBr may suggest that there are more interactions that occur between those ionic liquids compared to those of the chloride and acetate anions. The only one that is slightly different is that of the AMIMCl, which has a different cation group, compared to the others, with a carbon-carbon double bond attached to the imidazolium ring. This point may lead to another group that interacts with the cellulose or protein to be form. Finally, minimal differences were observed other than in the functional groups for the ionic liquids where those peaks vary between the 800 cm^{-1} to 400 cm^{-1} and in the alkene region seen in **Figure 3.2**.

Table 3.1. *Results of the β-sheet crystal fraction calculation with the corresponding Ionic liquids using FTIR amide I absorbance spectrum determined by Fourier transform self-deconvolution.*

Ionic liquid	Beta-Sheet Crystal Fraction
AMIMCl	31.0%
EMIMCl	37.1%
EMIMAc	39.2%
BMIMCl	37.5%
BMIMBr	58.6%
BMIMMeSO$_3$	58.9%

The percent of the crystal fraction was calculated in the Amide I regions of the ionic liquid that is presented in **Table 3.1**. This was performed to explain the shift that occurs from the **Figure 3.1** to **Figure 3.2** samples and to understand the changes in the anti-parallel β-sheet rearrangement. The points were deconvoluted using the amide I peaks corresponding to different levels of β- sheet configuration. The least squares method was used to match the deconvoluted spectra given [84]. The data provides information on the crystallinity of the silk material as a function of the ionic liquid. It was observed that the films with the chloride anion were the lowest in crystallinity, AMIMCl being the lowest with 31.0%, while BMIMCl and EMIMCl were 37.5% and 37.1% respectively. The EMIMAc was slightly more crystalline having a crystal fraction of 39.2%. This is relatively close to the EMIMCl. The BMIMBr and BMIMMeSO$_3$ are composed of the highest amount of crystallinity in the amide region with BMIMBr being 58.6% and BMIMMeSO$_3$ being 58.8%. The changes are correlated with the amount of interruption of the hydrogen bonding network, that naturally occurs between the amino acids in the anti-parallel β-sheet. The more the ionic liquids interacted with the natural polymers caused changes in the β-sheets, during the coagulation process a new conformation was formed in the β-sheet regions that resembled some of the original β-sheets configurations along with new orientations.

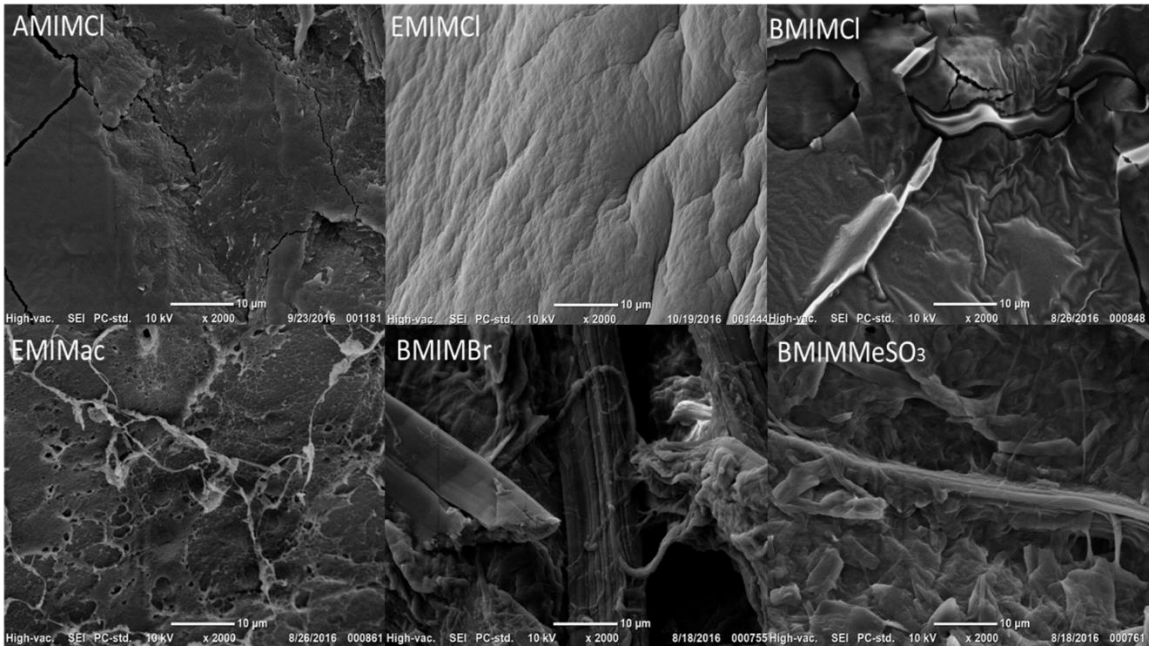

Figure 3.3*. SEM images of individual sections of the six ionic liquids regenerated film blends.*

Scanning Electron Microscopy (SEM) was used to characterize the topographical and morphological properties of the regenerated films, as shown in **Figure 3.3**. Blended films with a similar anion, exhibit a more uniform structure. This can be seen for the AMIMCl, BMIMCl and the EMIMCl topological images. A small difference is observed with the film regenerated from BMIMCl, which appears to be more rigid. Comparing ionic liquids with similar cations, EMIMCl and EMIMAc exhibited a difference in topological morphologies. The EMIMAc appears to have a porous structure. This could have occurred during the removal process of the ionic liquid causing channels to form as observed in the EMIMAc. The removal of the acetate anion group may be the reason for these particular porous marks. The BMIMBr and the $BMIMMeSO_3$ both appear to be very disorganized and fibrous like. The fibrous samples of bromide and methanesulfonate anion appear to have a greater impact on morphology creating a more string like layer than a solid flat surface. This enables us to conclude that the effect of the anion seems to play a greater role in the surface topology of the regenerated film sample than the cation does.

Table 3.2. *The TGA results are represented by the start and end temperature of decomposition. Along with the derivative value that yields the temperature when max decomposition occurs*

Sample	T_{Onset} (°C)	T_{End} (°C)	Wt. Loss (%)	$T_{\Delta Max}$ (°C)
Crystalline Cellulose	341.2	374.7	86.9	361.4
Mori Silk	294.9	357.9	60.9	329.9
AMIMCl	231.8	283.3	69.3	255.5
EMIMCl	259.4	301.5	80.2	289.2
EMIMAc	213.4	257.6	70.2	241.9
BMIMCl	252.6	298.4	91.3	282.8
BMIMBr	274.0	318.9	87.3	306.7
BMIMMeSO3	350.3	399.7	85.2	388.1

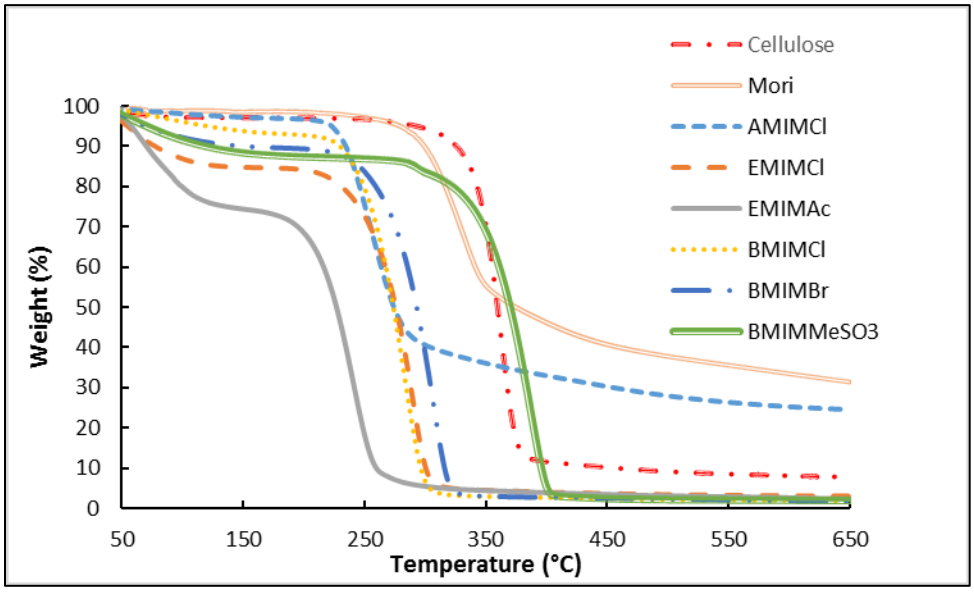

Figure 3.4. *Comparison of the thermograms of the film samples with the pure samples. The trends of the samples are observed along with the decomposition temperature (See table 3.2 for more details).*

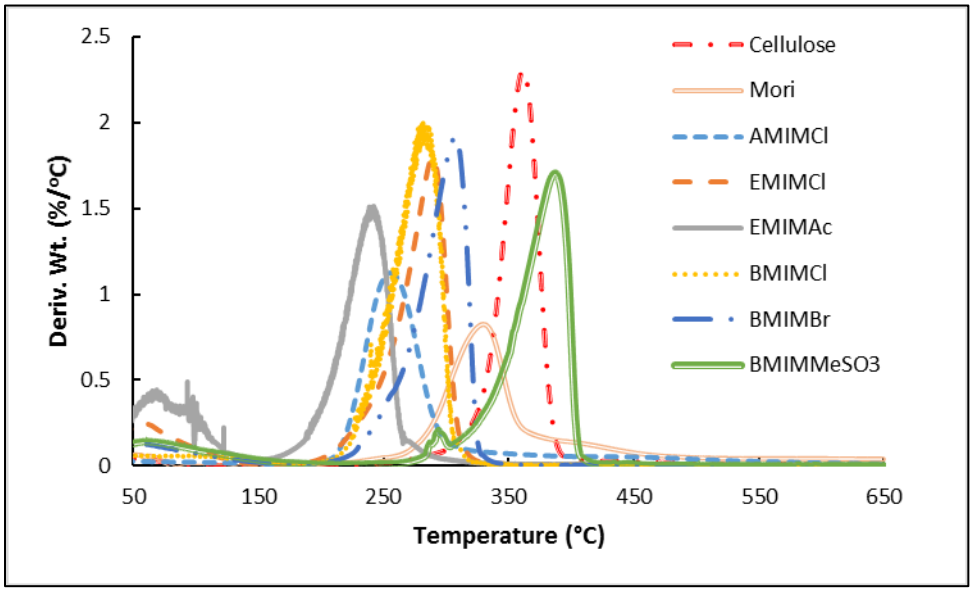

***Figure 3.5**. Derivative % weight loss plots comparing the peak temperature where majority of the decomposition occurs in the materials. (Refer to table 3.2 for more details).*

Figure 3.4 shows the thermograms for all blended samples. The first step in the comparison is to compare the regenerated films with cellulose and Mori silk. **Table 3.2** shows the differences between the two materials, as listed the onset temperature was at 341.2 °C for the cellulose and 294.9 °C for the silk. AMIMCl film showed the lowest temperature of degradation of 231.8 °C compared to similar anions, EMIMCl film and BMIMCl film at 259.4 °C and 252.6 °C respectively. The butyl and the ethyl groups seem to be in a closer range than the allyl group. The AMIMCl sample only decomposed about 69.3% of its weight and leveled off, while BMIMCl and EMIMCl films both decomposed 91.3% and 80.2%, respectively. The maximum decomposition occurred at 255.5 °C for the AMIMCl, for the EMIMCl occurred at 289.2 °C, and for the BMIMCl at 282.8 °C.

This information provides insight on how the cation group affects the overall thermal stability of the regenerated films. The film blended with AMIMCl behaves similarly to the decomposition of the Mori silk, as it has a peak that does not fully decompose (like the other ionic liquid films). This indicates that the silk has more control over the AMIMCl, possibly with the allyl group interacting with the silk molecule stronger than with cellulose. Comparisons between similar cations can be made between the

EMIMAc and the EMIMCl. The EMIMAc in general had a lower onset of weight loss 213.4 °C and lower maximum decomposition 241.9 °C as seen in **Table 3.2** and **Figure 3.5**. The EMIMAc film exhibits the lowest thermal stability compared to the rest of the ionic liquids. The EMIMCl film decomposition starting temperature was about 40 °C higher than the EMIMAc film. This shows that there is more of a dependency on the anion rather than the cation. The last two ionic liquids were the BMIMBr and the $BMIMMeSO_3$. Both of the ionic liquids films prove to have higher stability than that of the chloride anions 274.0 °C and 350.3 °C, respectively. This agrees with the percent β-sheet crystallization calculation which demonstrated that these two samples had higher percent crystallinity. This in comparison shows that the more interaction sites of the bulkier anions this may allow for a more thermally stable film to be formed. This data is in agreement with other published reports as the thermal properties were explored for the ionic liquids individually [79]. The ionic liquid plays a major role in the properties of the film seen in the FTIR data. Interestingly, the film blended with $BMIMMeSO_3$ has a higher decomposition temperature than the pure cellulose and silk components, suggesting that the anion is strongly interacting with both the cellulose and the ionic liquids. The various results provides evidence to suggest that the ionic liquid can increase overall thermal stability [79]. The information gathered from the thermal analysis enable us to suggest that an increase in molecular interaction influences the overall thermal stability.

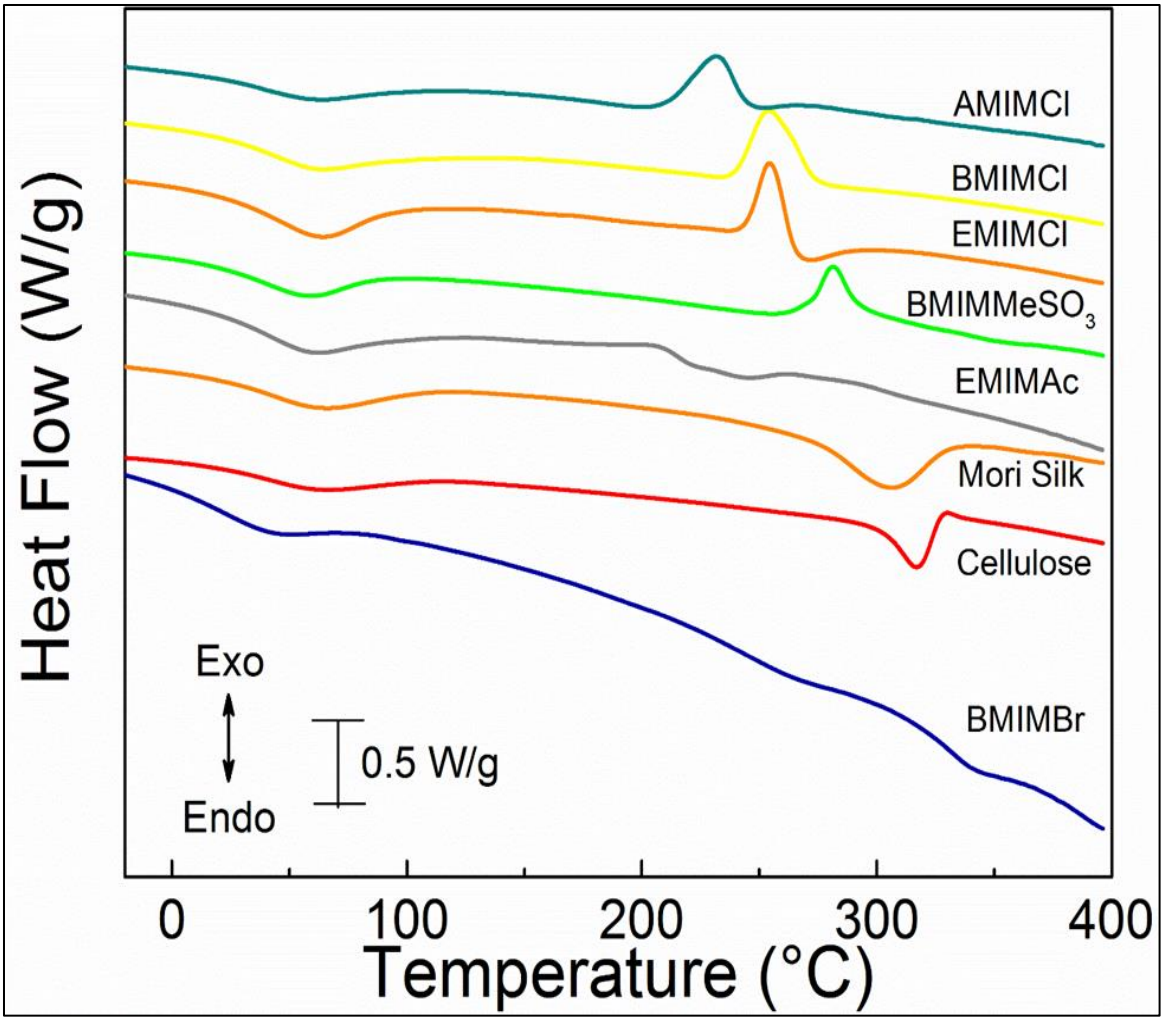

***Figure 3.6**. Standard DSC scans of the silk and cellulose composite films with 10 wt% silk and 90 wt% cellulose made from different ionic liquids. (In descending order, AMIMCl, BMIMCl, EMIMCl, $BMIMMeSO_3$, EMIMAc, Mori silk, Cellulose and BMIMBr). The samples were heated at 2 °C/min from -30 to 400 °C.*

As shown in **Figure 3.6**, standard DSC is used to study the thermal properties of the composite films. For all the six samples, there is an endothermic peak for each between 40-100 °C, which is a blend-bound solvent transition peak. It can be explained that the solvent evaporates just after the glass transition [20, 85]. For pure cellulose, it has an endothermic peak at 321 °C, which is mainly attributed to the depolymerization of cellulose. Then, there is a small exothermic peak, which is due to the charring process [86]. The degradation peak of Mori silk showed up around 312 °C. Thereafter, for AMIMCl,

BMIMCl, EMIMCl, $BMIMMeSO_3$ and EMIMAc ionic liquid films, each sample has an exothermic peak, which is a strong non-isothermal crystallization peak for cellulose. For AMIMCl film, the composite has a crystallization peak centered at 228 °C; for BMIMCl and EMIMCl films, the composite films have a crystallization peak centered at 252 °C. However, compared with the peak of BMIMCl film, the crystallization peak of EMIMCl film is sharper, which means that the composite films prepared using EMIMCL method is easier to crystallize. For the $BMIMMeSO_3$ film, the composite film prepared through this method has the highest crystallization temperature with a crystallization peak centered at 286 °C. For the EMIMAc film, there is a weak exothermic peak centered at 207 °C. For the BMIMBr film, there is a broad exothermic halo centered at 317 °C. The crystallization temperature of the composite films varies with different fabrication method, this can be explained due to the different ionic liquid resulting in different structures in the composite films, which is confirmed by the SEM figures. At the same time, the degradation temperature of all the composite films manufactured from ionic liquid method decreased when compared with the pure cellulose. There is only one crystallization peak observed in the composite films in **Figure 3.6**, and this indicates that silk and cellulose were well-blended to a homogeneous system without immiscibility. After the crystallization peak, all the samples show an endothermic peak, which is caused by the degradation of silk component [87].

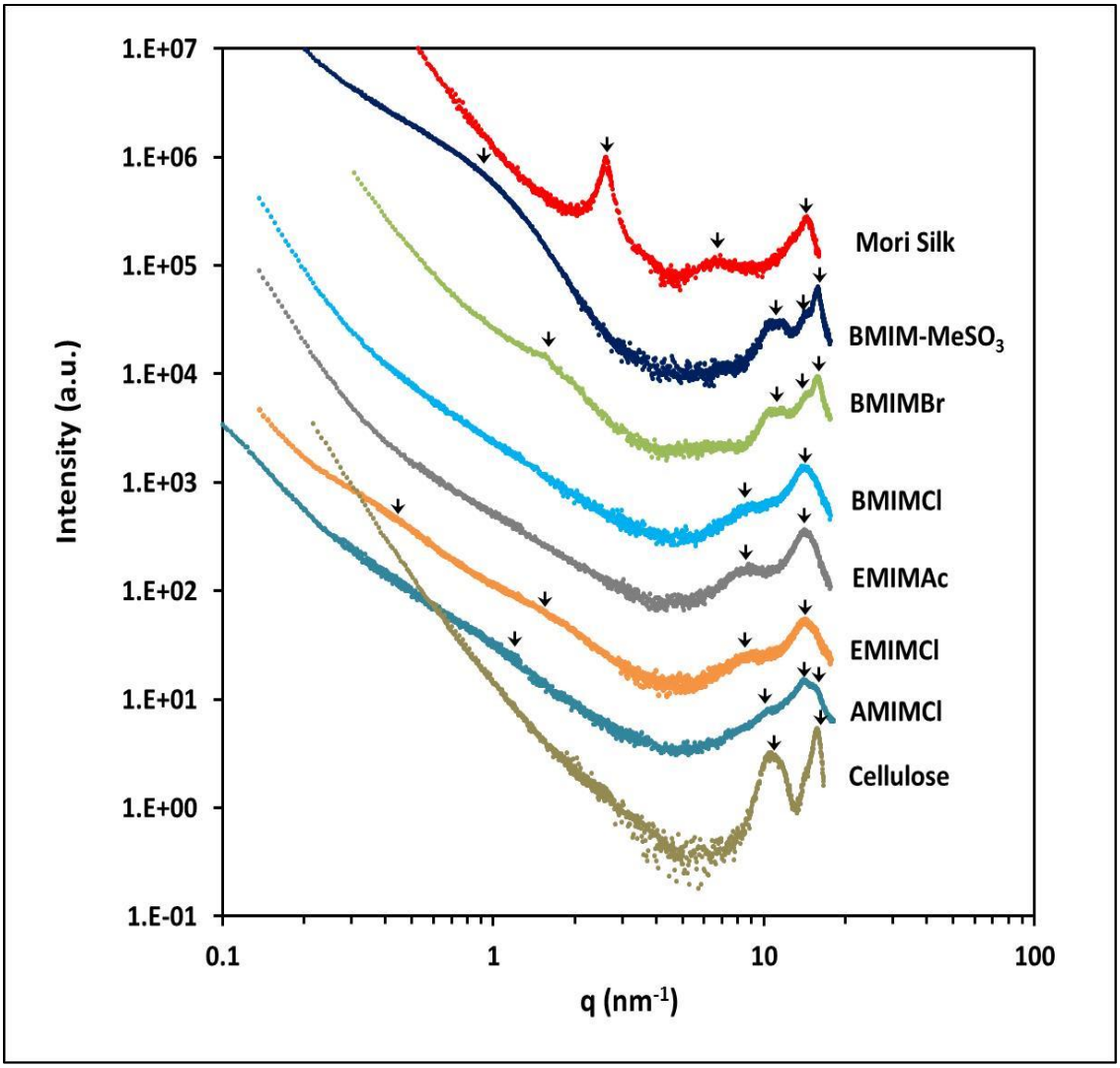

Figure 3.7*: X-ray scattering profiles as a function of ionic liquids type. The intensity is offset to be able to distinguish between the various scatterings. The arrows indicated the position of the main peaks.*

X-ray scattering was then used to probe the morphology of the raw materials. The pure components and the regenerated films are comprised of varying ionic liquids over a wide range of scattering angles. **Figure 3.7** shows the scattering profiles of each sample recorded at room temperature. The selected samples were chosen to look at morphological variations as a function of ionic liquid type. We initiate our morphological investigation by looking at distinct spacing observed in cellulose. In cellulose, two distinct spacings are observed. The spacings in cellulose can be attributed to its crystalline regions (q_1=15.75

nm^{-1} and q_2=10.61 nm^{-1}). Between q_1 and q_2, there are two slightly notable shoulders at q_a=14.22 nm^{-1}, and q_b= 11.9 nm^{-1}. The d-spacings are d_1 of 0.40 nm, d_2 of 0.60 nm, d_a of 0.44 nm, and d_b of 0.53 nm, which are related to the monoclinic unit cell of cellulose I_β equatorial lattice planes. In support of our data, Vainio *et al* reported crystalline monoclinic cellulose of Avicel given reflection at 2θ values of 14.6° $(1\bar{1}0)$, 16.6° (110) and 22.4° (200) [61]. Similar results were reported by Helbert, where he showed a high resolution image of the cross-sectioned *Halocynthia papillosa* microcrystal [10]. The 0.44 nm is related to the layer in lateral direction or 102 and 012 reflections. For the silk fibers, we observed three scattering vector peaks at q_1=14.50 nm^{-1}, q_2=6.60 nm^{-1}, and q_3=2.62 nm^{-1}. The d-spacing, for each peak used the formula $d=2\pi/q$ formula, for these scattering peaks are d_1=0.43 nm, d_2=0.95 nm, and d_3=2.40 nm. The d-spacing observed at 0.44 nm corresponds to the distance between β-strands, the distance at 0.95 nm corresponds to the inter-sheet distance between β-sheets, and the distance at 2.40 nm corresponds to the size of the β-sheets in the lateral direction [54-60]. Upon further inspection, there is a weak peak at q_a=12.65 nm^{-1} with a d-spacing of d_a=0.50 nm. This peak corresponds to the distance between β-strand oriented perpendicular to the fiber.

The scattering profile for 10% silk made from AMIMCl provided information on four main characteristic spacings: q_1= 15.72 nm^{-1}, q_2= 14.20 nm^{-1}, q_3= 10.30 nm^{-1}, and q_4= 1.30 nm^{-1} . The d-spacing for each peak is d_1 = 0.40 nm, d_2 = 0.44 nm, d_3 = 0.61 nm, and d_4 = 4.83 nm, respectively. The scattering spacing confirms the presence of the various macromolecules in the new regenerated biopolymer. It clearly shows the crystalline regions of cellulose (q_1= 15.72 nm^{-1}) as well as the silk (q_2= 14.20 nm^{-1}) as compared to the pure samples. Other regions (q_3= 10.30 nm^{-1} and q_4= 1.30 nm^{-1}) correlate between both species. The former corresponds to the inter-sheet distance and the latter is related to the interaction between the cellulose microfibril and the β-sheets of silk. These results suggest that the cellulose molecules are interacting with the silk molecules and affecting the microfibril region possibly via hydrogen bonds. The lack of a clear periodicity prevents us from confirming specific conformation. As the imidazolium ring's functional group changed from allyl to ethyl with a similar counterion, the scattering confirms the presence of four characteristics spacings: q_1= 14.38 nm^{-1}, q_2= 8.70 nm^{-1}, q_3= 1.60 nm^{-1}, and q_4= 0.460 nm^{-1}. The d-spacing for each peak is d_1 = 0.44 nm, d_2 = 0.72 nm, d_3 = 3.92 nm, and d_4 = 13.65

nm, respectively. The high scattering vector peak is related to the amorphous nature of this polymer blend. The inter-sheet distance increases from 0.61 nm to 0.72 nm as the side chain of the imidazolium changed from allyl to ethyl. This appears to suggest that the allyl group in the ionic liquid affects the recrystallization and the inter-sheet distance of the polymer blend. Both peaks located at low angle scattering vector suggest possible microphase separation. The scattering peak at 1.60 nm^{-1} could be related to the β-sheets lateral distance and the one at q_4= 0.460 nm^{-1} could be related to the cellulose microfibril. These two peaks are not observed when the imidazolium side chain increases from ethyl to butyl or when the counter ion changes from chloride to acetate. For both of these polymer blends, EMIMAc and BMIMCl, the X-ray scattering showed two characteristics spacings: q_1= 14.38 nm^{-1} (d_1 = 0.44 nm) and q_2= 8.70 nm^{-1} (d_2 = 0.72 nm). The high scattering vector suggests an amorphous morphology for both samples. While the scattering peaks are similar, the EMIMAc showed increase in broadness for each peak, suggesting the effect of an increase in interaction due to the acetate ions. The X-ray scattering for BMIMBr and $BMIMMeSO_3$ showed similar scattering vector at high vector region with q_1= 15.75 nm^{-1} (d_1 = 0.40 nm), q_2= 14.50 nm^{-1} (d_2 = 0.43 nm) and q_3= 11.10 nm^{-1} (d_2 = 0.53 nm). The high vector region is different from the previous samples. The sharpness of the peak suggests a semicrystalline morphology for these two samples. One could easily observe the peak associated with cellulose and silk. Interestingly, these two samples have two different scattering peaks at low vector regions. The BMIMBr has a peak at q= 1.58 nm^{-1} (d = 3.97 nm) and $BMIMMeSO_3$ at q= 0.888 nm^{-1} (d = 7.07 nm). The scattering peak for $BMIMMeSO_3$ is pronounced, suggesting possible micro-phase separation. This region is related to the intermolecular interaction between the cellulose microfibril, silk β-sheets in the lateral direction and the ionic liquid.

3.4 Conclusion:

The results provided evidence that the regenerated films were successfully made from all the ionic liquids. All blended films were homogenous as confirmed via DSC. The various ionic liquid film blends each exhibited similar IR structures to that of the silk and cellulose structure, helping confirm a blended polymer film. These changes are observed in the shifts in the amide peaks, also in the reduction in the peaks that corresponded with

the ionic liquids. Also, observed in the FTIR was the crystal fraction of the amide I region indicating that the larger anions had an increase in percent crystallinity of β-sheets. The X-Ray scattering study confirmed the amorphous and semicrystalline regions as seen in the crystal fraction calculations with the corresponding samples, along with showing the semicrystalline regions in the $BMIMMeSO_3$ and the BMIMBr blended films. The spacing differences in the ionic liquids show a relationship between the intermolecular interactions. The differences in the topology were observed as the ionic liquids with the chloride anion group appeared to be more uniform unlike those of the bromide or the methanesulfonate groups, which appear to be more amorphous. The EMIMAc film appeared to be more porous material, with pores most likely from channels caused from the removal process of the ionic liquid. The thermal analysis gives insight on the type of conditions that the regenerated films can be used in. Since the films using BMIMBr and $BMIMMeSO_3$ with different anion groups appear to be more thermally stable compared to the other films, this can be due to additional interaction points of the anion which allows for a more semicrystalline structure. The AMIMCl film has similar decomposition to that of the Mori silk, thus providing evidence that the allyl functional group provides a different interaction with the Mori silk unlike the other ionic liquids. Slight changes in the 10% silk films based on the cation groups were observed, as shown for the butyl, ethyl, and allyl cation functional groups. Additionally, the films prepared using various ionic liquids have different corresponding T_g values, confirming the various observations of different structures shown on the SEM.

CHAPTER 4

Conclusion and Future Studies

4.1 Conclusion

The ionic liquids dissolution process allowed for the cellulose and the Mori silk to fully dissolve and reform into a blended film. The first study involved exploring the relationship between silk/cellulose concentration using AMIMCl as the solvent and water as the coagulating agent. The regenerated blended films were more stable at a lower concentration of silk where the films were more resilient and firm. The topology of the films exhibited changes in pattern as a function of silk content. At low silk concentration, the films were uniform, while at high silk concentration the films were disorganized exhibiting no pattern. The thermal properties also were affected due to the function of silk content, allowing for a homogenous blended material to be formed. The X-ray scattering confirmed that there are variations in the morphology of the structures relating to the silk content. Blended films formed into different configurations depending on the silk content, and films were either intermediate semicrystalline or amorphous. 10% cellulose and 90% silk samples did not exhibit a transformation from cellulose I to cellulose II, however, an intermediate crystalline structure was seen that had properties of both silk and cellulose I. Possible reason for this is that the reordered silk is being oriented in a face to face manner from the reordering of the polypeptide chains. An alteration of the cellulose microfibril was also observed due to the addition of the silk.

The interactions between the silk and the cellulose dissolution and regeneration showed that the silk altered the cellulose structure, and this alteration caused changes in the formation of β-sheets. In particular, cellulose microfibril formation was affected by silk β-sheets. These various morphological changes cause disruption in the thermal properties of the blended materials. The hydrogen bonding that normally occurs between the silk and the cellulose were disrupted due to the chloride ion interactions. The increase of the silk ratio appeared to cause more interactions to occur on the silk itself rather than interacting with the cellulose, giving a less stable regenerated film. The results showed the possibility of preparing tunable properties, because the cellulose/silk proportions can be adjusted to optimize the desired properties by tuning the level of crystallization in the film.

The second study focused on the physicochemical effects as a function of ionic liquid type. The concentration of the silk and cellulose were kept constant as the films were composed of 90% ionic liquid and 10% biomaterial. Structural changes were observed by means of the FTIR characterization result showing shifts in the amide peaks and in the reduction in the peaks height that correspond with the ionic liquids. The chloride anions had a more uniform topology as compared to the bromide and methansulfonate blended films. The EMIMAc films appeared to be a porous material caused from the removal process of the ionic liquid causing channels to be formed. Thermal analysis gives information on the regenerated film samples demonstrating the effect of cations such as the butyl, ethyl, and allyl cation functional groups which appeared to have little changes on the thermal stability. The BMIMBr and $BMIMMeSO_3$ films had a higher level of thermal stability due to an increased number of possible interaction points. Bromide having more electrons allows for more disruption in the hydrogen bonding of the cellulose and silk. Similarly, methanesulfonate has a very resonant structure, allowing it to be more stable. This resonate structure also allows for more interaction points to occur on the oxygen allowing for hydrogen bonding. The DSC confirmed that all blended films were homogenous. The information showed unique T_g information for each ionic liquid blended film and allowed for a comparison to be made with the SEM. The X-Ray scattering study confirms the amorphous regions seen in the SEM with the corresponding samples. The bromide and methanesulfonate films both have semicrystalline areas, affecting the spacing observed in the X-Ray scattering data of the regenerated films. This confirms that the different molecular spacings have a relationship to interaction and morphology. The crystal fraction of the amide I region calculated from the FTIR confirm these patterns in the X-ray scattering supporting the conclusion that the larger anions correlated with an increase in crystallinity of β-sheets. The small percentage of silk with cellulose resulted in a disruption allowing for cellulose to recrystallize as an intermediate structure resembling cellulose I. The cellulose intermediate structure variability is due to many factors, including the type of ionic liquid, constraints of large molecules, and the disruption of the crystalline structure. This in turn shows a correlation between the inter-and intramolecular interactions to be affected greatly by the anion, and to a much lesser degree by the cation.

The AMIMCl film has similar decomposition to that of the Mori silk film, thus providing evidence that the allyl functional group may interact differently with the Mori silk unlike the other ionic liquids. The interactions that occur with the cation play a small role in the films over all morphology as the compared samples have small changes in the films stability. The level of disruption that the anion causes between the cellulose and the silk allows for structural and thermal complexities in the regenerated blended films.

4.2 Future Studies

The coagulation process is a point of interest as it allows for the blended film to form. Future studies can explore the effects of different coagulation temperature of the water on the regenerated films. Water removes the ionic liquid from the film sample, and the temperature controlled coagulation process may provide insight on the time of removal or interactions that are occurring. The ability to speed up the removal process is important, for both industry and medical fields. It would allow for a shorter process of coagulation and allow for more focus on the biomaterial made, In the first study, the time was 30 minutes, and that showed that some ionic liquid was still trapped in the film samples. In the other study, the films were kept in water for 48 hours and that removed most of the ionic liquid seen in the FTIR spectra. Removal of the ionic liquid is pertinent, depending on the use of the films, as the ionic liquids can have negative effects. Along with showing a decrease in the ionic liquid observed to be trapped in the blended film, a difference on the morphological structures was demonstrated. For example, at 30 minutes, the films exhibited a grainy/spherical morphology but as the coagulation time was increased from 30 minutes to 48 hours, a less grainy/spherical structure were created. The spatiotemporal changes will need to be further explored with different coagulation times and temperature to fully understand these interactions. The effects on the film during the coagulation process are not as explored and more information will be beneficial for studying the overall film properties. Continued studies can be explored by using an atomic force microscope to see other topological changes.

Another interest is using different coagulating agents to regenerate the films. The coagulator that is used needs a point of interaction to occur with cellulose and silk and will not harm the materials being regenerated. Along with the ability of removing the ionic

liquid and changing the interaction process, the coagulator can be combined with different liquids. One example of a different coagulator would be using methanol. Preliminary experiments using methanol as a coagulator showed an increase the β-sheet formation of the blended films. In some cases, allowing for a combined coagulation agent, such as water and methanol, can create a film that has properties that are desired for strength or certain structure. The way the coagulator interacts with the solution to regenerate the film is important in controlling the films properties. It can help explain the formation and patterns in the film samples or improve the removal of the ionic liquid. More studies with various coagulators should be done to understand possible effects and outcomes of the regenerated film blend. Ideally, a series of experiments will be set up with various times (for example 1, 24, and 48 hours) with a mixture of water/alcohol at various concentrations (for example: 10%, 50%, 90%) and various temperatures (for example: 25, 38, 50, 75°C). Using similar protein and cellulose concentrations as the comparison to the other experiments will allow for a monitoring of the morphology, structure, and chemical composition. Expected outcome is to see in an increase in the β-sheet formation as a function of protein and water/alcohol content. This will hopefully lead to controlling the recrystallization process.

Supplemental Material

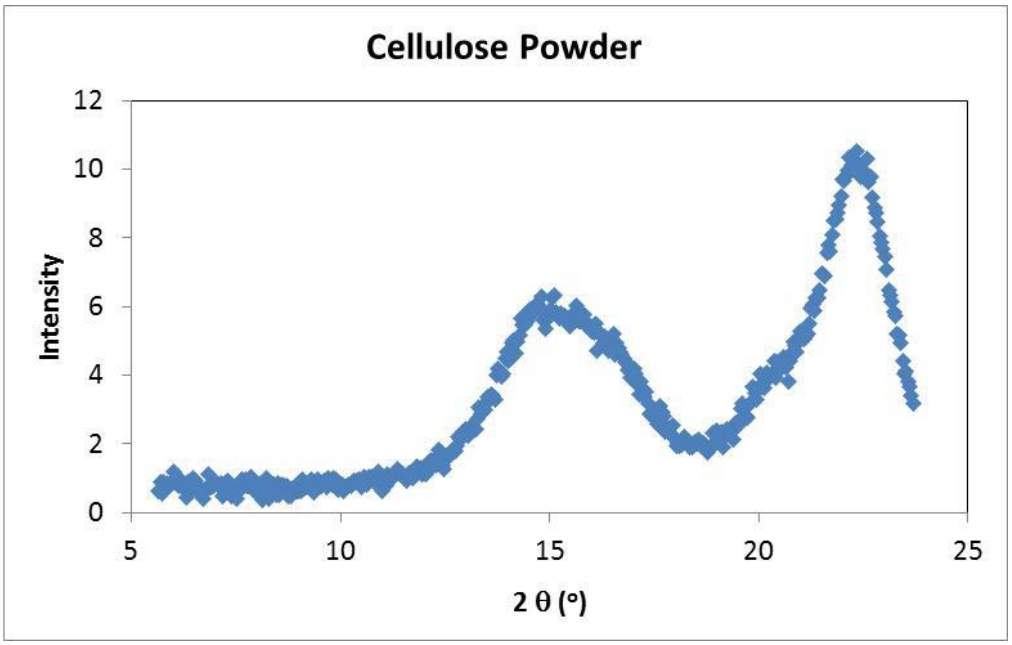

Figure S1: Cellulose Powder (Avicel) X-ray scattering profile for the Wide Angle Region as a function of 2θ

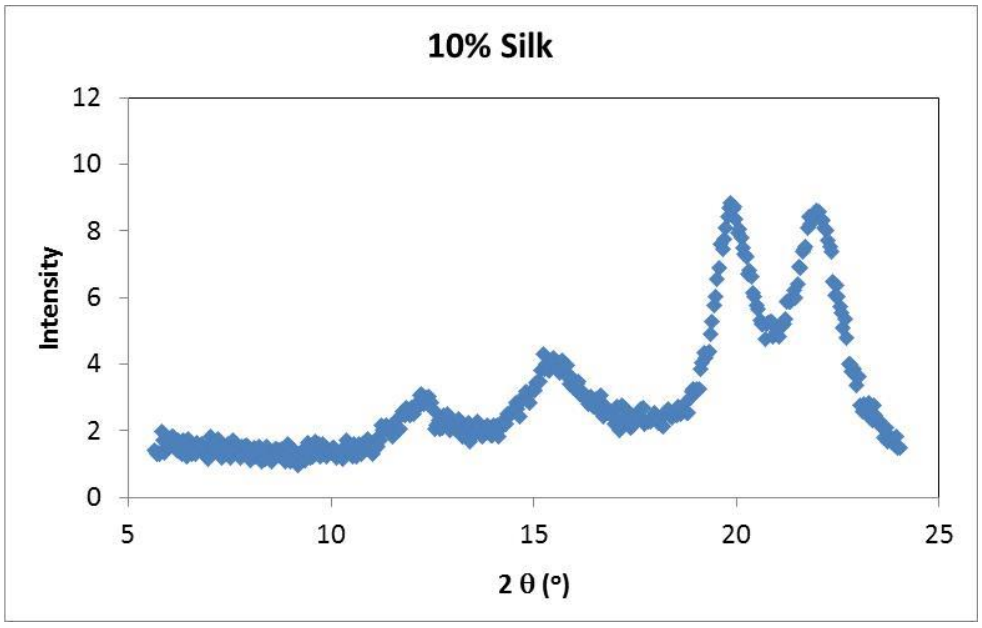

Figure S2: 10% Silk Films X-ray scattering profile for the Wide Angle Region as a function of 2θ

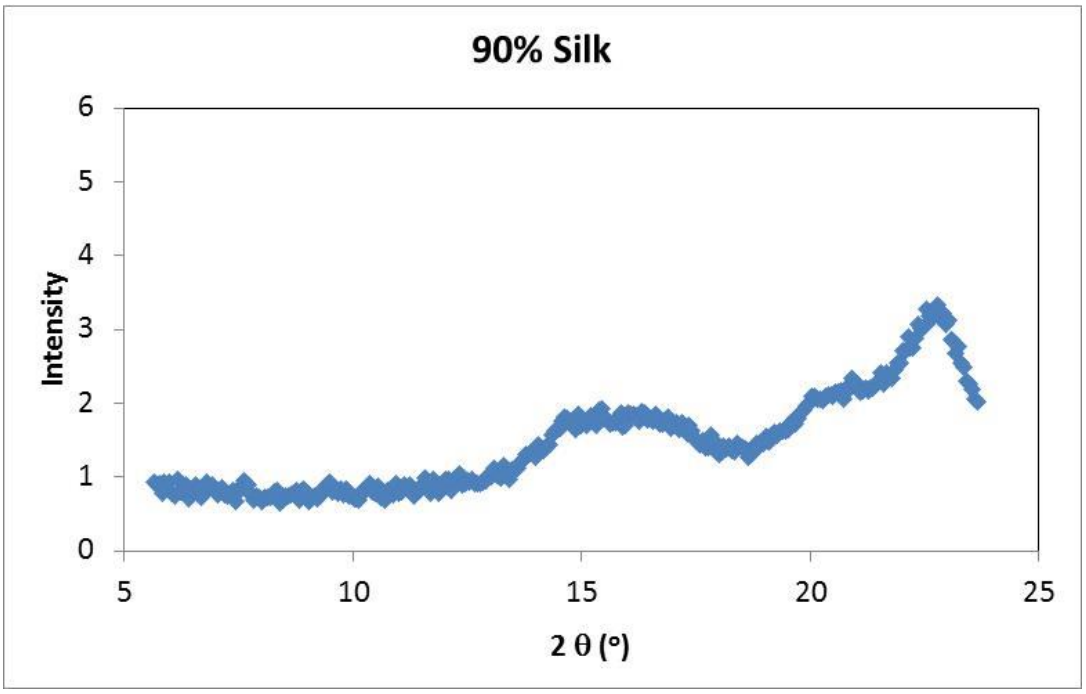

Figure S3: 90% Silk Films X-ray scattering profile for the Wide Angle Region as a function of 2θ.

References

1. Ratner, Buddy D, Hoffman, Allan S, Schoen, Frederick J, and Lemons, Jack E, *Biomaterials science: a multidisciplinary endeavor.* Biomaterials science: an introduction to materials in medicine (2nd ed.) Elsevier Science & Technology, Oxford, 2004: p. 1-9.

2. Yin, Jinghua and Luan, Shifang, *Opportunities and challenges for the development of polymer-based biomaterials and medical devices.* Regenerative Biomaterials, 2016. **3**(2): p. 129-135.

3. Metzke, M. and Guan, Z., *Structure-property studies on carbohydrate-derived polymers for use as protein-resistant biomaterials.* Biomacromolecules, 2008. **9**(1): p. 208-15.
4. Suh, Hwal, *Recent advances in biomaterials.* Yonsei Medical Journal, 1998. **39**: p. 87-96.

5. Hsu, Shan-hui, Hung, Kun-Che, and Chen, Cheng-Wei, *Biodegradable polymer scaffolds.* Journal of Materials Chemistry B, 2016. **4**(47): p. 7493-7505.

6. Suh, J-K Francis and Matthew, Howard WT, *Application of chitosan-based polysaccharide biomaterials in cartilage tissue engineering: a review.* Biomaterials, 2000. **21**(24): p. 2589-2598.

7. Liu, Jun, Willför, Stefan, and Xu, Chunlin, *A review of bioactive plant polysaccharides: Biological activities, functionalization, and biomedical applications.* Bioactive Carbohydrates and Dietary Fibre, 2015. **5**(1): p. 31-61.

8. Ghazarian, Haike, Idoni, Brian, and Oppenheimer, Steven B, *A glycobiology review: carbohydrates, lectins and implications in cancer therapeutics.* Acta histochemica, 2011. **113**(3): p. 236-247.

9. Gorelik, Elieser, Galili, Uri, and Raz, Avraham, *On the role of cell surface carbohydrates and their binding proteins (lectins) in tumor metastasis.* Cancer and Metastasis Reviews, 2001. **20**(3-4): p. 245-277.

10. Helbert, William, Nishiyama, Yoshiharu, Okano, Takeshi, and Sugiyama, Junji, *Molecular Imaging of Halocynthia papillosa Cellulose.* Journal of structural biology, 1998. **124**(1): p. 42-50.

11. Yuan, Xueming and Cheng, Gang, *From cellulose fibrils to single chains: understanding cellulose dissolution in ionic liquids.* Physical Chemistry Chemical Physics, 2015. **17**(47): p. 31592-31607.

12. Sundberg, Johan, Toriz, Guillermo, and Gatenholm, Paul, *Effect of xylan content on mechanical properties in regenerated cellulose/xylan blend films from ionic liquid.* Cellulose, 2015. **22**(3): p. 1943-1953.

13. Atalla, Rajai H. and Vanderhart, David L., *Native Cellulose: A Composite of Two Distinct Crystalline Forms.* Science, 1984. **223**(4633): p. 283-285.

14. Zhang, Jinming, Xu, Lili, Yu, Jian, Wu, Jin, Zhang, Xiaoyu, He, Jiasong, and Zhang, Jun, *Understanding cellulose dissolution: effect of the cation and anion structure of ionic liquids on the solubility of cellulose.* Science China Chemistry, 2016. **59**(11): p. 1421-1429.

15. Reddy, K Obi, Maheswari, C Uma, Dhlamini, MS, Mothudi, BM, Zhang, Jinming, Zhang, Jun, Nagarajan, Rajini, and Rajulu, A Varada, *Preparation and characterization of regenerated cellulose films using borassus fruit fibers and an ionic liquid.* Carbohydrate Polymers, 2016. **160**: p. 203-211.

16. Poletto, Matheus, Ornaghi, Heitor L, and Zattera, Ademir J, *Native cellulose: structure, characterization and thermal properties.* Materials, 2014. **7**(9): p. 6105-6119.

17. Wegst, Ulrike GK, Bai, Hao, Saiz, Eduardo, Tomsia, Antoni P, and Ritchie, Robert O, *Bioinspired structural materials.* Nature materials, 2015. **14**(1): p. 23-36.

18. Hu, Xiao, Cebe, Peggy, Weiss, Anthony S., Omenetto, Fiorenzo, and Kaplan, David L., *Protein-based composite materials.* Materials Today, 2012. **15**(5): p. 208-215.

19. Altman, Gregory H, Diaz, Frank, Jakuba, Caroline, Calabro, Tara, Horan, Rebecca L, Chen, Jingsong, Lu, Helen, Richmond, John, and Kaplan, David L, *Silk-based biomaterials.* Biomaterials, 2003. **24**(3): p. 401-416.

20. Hu, Xiao, Kaplan, David, and Cebe, Peggy, *Dynamic protein− water relationships during β-sheet formation.* Macromolecules, 2008. **41**(11): p. 3939-3948.

21. Hu, Xiao, Raja, Waseem K., An, Bo, Tokareva, Olena, Cebe, Peggy, and Kaplan, David L., *Stability of Silk and Collagen Protein Materials in Space.* Scientific Reports, 2013. **3**: p. 3428.

22. Freddi, Giuliano, Romanò, Maria, Massafra, Maria Rosaria, and Tsukada, Masuhiro, *Silk fibroin/cellulose blend films: preparation, structure, and physical properties.* Journal of Applied Polymer Science, 1995. **56**(12): p. 1537-1545.

23. Isogai, A and Atalla, RH, *Dissolution of cellulose in aqueous NaOH solutions.* Cellulose, 1998. **5**(4): p. 309-319.

24. Pham, Thi Phuong Thuy, Cho, Chul-Woong, and Yun, Yeoung-Sang, *Environmental fate and toxicity of ionic liquids: a review.* Water research, 2010. **44**(2): p. 352-372.

25. Zhang, Hao, Wu, Jin, Zhang, Jun, and He, Jiasong, *1-Allyl-3-methylimidazolium chloride room temperature ionic liquid: a new and powerful nonderivatizing solvent for cellulose.* Macromolecules, 2005. **38**(20): p. 8272-8277.

26. Pang, Jin-Hui, Liu, Xin, Wu, Miao, Wu, Yu-Ying, Zhang, Xue-Ming, and Sun, Run-Cang, *Fabrication and characterization of regenerated cellulose films using different ionic liquids.* Journal of Spectroscopy, 2014. **2014**: p. 8.

27. Phillips, David M, Drummy, Lawrence F, Conrady, Deborah G, Fox, Douglas M, Naik, Rajesh R, Stone, Morley O, Trulove, Paul C, De Long, Hugh C, and Mantz, Robert A, *Dissolution and regeneration of Bombyx mori silk fibroin using ionic liquids.* Journal of the American Chemical Society, 2004. **126**(44): p. 14350-14351.

28. Pinkert, André, Marsh, Kenneth N., Pang, Shusheng, and Staiger, Mark P., *Ionic Liquids and Their Interaction with Cellulose.* Chemical Reviews, 2009. **109**(12): p. 6712-6728.

29. Kosan, Birgit, Michels, Christoph, and Meister, Frank, *Dissolution and forming of cellulose with ionic liquids.* Cellulose, 2008. **15**(1): p. 59-66.

30. Wang, Qin, Yang, Yuhong, Chen, Xin, and Shao, Zhengzhong, *Investigation of rheological properties and conformation of silk fibroin in the solution of AmimCl.* Biomacromolecules, 2012. **13**(6): p. 1875-1881.

31. Abdul Khalil, H. P. S., Bhat, A. H., Abu Bakar, A., Tahir, Paridah Md., Zaidul, I. S. M., and Jawaid, M., *Cellulosic Nanocomposites from Natural Fibers for Medical Applications: A Review*, in *Handbook of Polymer Nanocomposites. Processing, Performance and Application: Volume C: Polymer Nanocomposites of Cellulose Nanoparticles*, K.J. Pandey, et al., Editors. 2015, Springer Berlin Heidelberg: Berlin, Heidelberg. p. 475-511.

32. Cheng, Gang, Varanasi, Patanjali, Li, Chenlin, Liu, Hanbin, Melnichenko, Yuri B., Simmons, Blake A., Kent, Michael S., and Singh, Seema, *Transition of Cellulose Crystalline Structure and Surface Morphology of Biomass as a Function of Ionic Liquid Pretreatment and Its Relation to Enzymatic Hydrolysis.* Biomacromolecules, 2011. **12**(4): p. 933-941.

33. Samayam, Indira P., Hanson, B. Leif, Langan, Paul, and Schall, Constance A., *Ionic-Liquid Induced Changes in Cellulose Structure Associated with Enhanced Biomass Hydrolysis.* Biomacromolecules, 2011. **12**(8): p. 3091-3098.

34. Zhou, Liang, Wang, Qin, Wen, Jianchuan, Chen, Xin, and Shao, Zhengzhong, *Preparation and characterization of transparent silk fibroin/cellulose blend films.* Polymer, 2013. **54**(18): p. 5035-5042.

35. Thomas, Lynne H., Forsyth, V. Trevor, Martel, Anne, Grillo, Isabelle, Altaner, Clemens M., and Jarvis, Michael C., *Diffraction evidence for the structure of cellulose microfibrils in bamboo, a model for grass and cereal celluloses.* BMC Plant Biology, 2015. **15**(1): p. 1-7.

36. Agarwal, Umesh P., *Raman imaging to investigate ultrastructure and composition of plant cell walls: distribution of lignin and cellulose in black spruce wood (Picea mariana).* Planta, 2006. **224**(5): p. 1141-1153.

37. Levy, Ilan, Nussinovitch, Amos, Shpigel, Etai, and Shoseyov, Oded, *Recombinant cellulose crosslinking protein: a novel paper-modification biomaterial.* Cellulose, 2002. **9**(1): p. 91-98.

38. Su, Jun-Feng, Huang, Zhen, Yuan, Xiao-Yan, Wang, Xin-Yu, and Li, Min, *Structure and properties of carboxymethyl cellulose/soy protein isolate blend edible films crosslinked by Maillard reactions.* Carbohydrate Polymers, 2010. **79**(1): p. 145-153.

39. Tomczyńska-Mleko, Marta, Terpiłowski, Konrad, and Mleko, Stanisław, *Physicochemical properties of cellulose/whey protein fibers as a potential material for active ingredients release.* Food Hydrocolloids, 2015. **49**: p. 232-239.

40. Isogai, A. and Atalla, R. H., *Dissolution of Cellulose in Aqueous NaOH Solutions.* Cellulose, 1998. **5**(4): p. 309-319.

41. Wang, Qin, Chen, Quan, Yang, Yuhong, and Shao, Zhengzhong, *Effect of Various Dissolution Systems on the Molecular Weight of Regenerated Silk Fibroin.* Biomacromolecules, 2013. **14**(1): p. 285-289.

42. Zhang, Hao, Wu, Jin, Zhang, Jun, and He, Jiasong, *1-Allyl-3-methylimidazolium Chloride Room Temperature Ionic Liquid: A New and Powerful Nonderivatizing Solvent for Cellulose.* Macromolecules, 2005. **38**(20): p. 8272-8277.

43. Johnson, K. E., *What's an ionic liquid?* Electrochemical Society Interface, 2007. **16**(1): p. 38-41.

44. Yoshizawa, Masahiro and Ohno, Hiroyuki, *Anhydrous proton transport system based on zwitterionic liquid and HTFSI.* Chemical Communications, 2004(16): p. 1828-1829.

45. Fukushima, Takanori, Asaka, Kinji, Kosaka, Atsuko, and Aida, Takuzo, *Fully Plastic Actuator through Layer-by-Layer Casting with Ionic-Liquid-Based Bucky Gel.* Angewandte Chemie, 2005. **117**(16): p. 2462-2465.

46. Tang, Jianbin, Tang, Huadong, Sun, Weilin, Radosz, Maciej, and Shen, Youqing, *Poly(ionic liquid)s as new materials for CO2 absorption.* Journal of Polymer Science Part A: Polymer Chemistry, 2005. **43**(22): p. 5477-5489.

47. Thuy Pham, Thi Phuong, Cho, Chul-Woong, and Yun, Yeoung-Sang, *Environmental fate and toxicity of ionic liquids: A review.* Water Research, 2010. **44**(2): p. 352-372.

48. Wang, Xuejing, Li, Huiquan, Cao, Yan, and Tang, Qing, *Cellulose extraction from wood chip in an ionic liquid 1-allyl-3-methylimidazolium chloride (AmimCl).* Bioresource Technology, 2011. **102**(17): p. 7959-7965.

49. Scherrer, P, *Determination of size on the internal structure of colloid particles by means of X-ray beams.* Nachr. Ges. Wiss. GSttingen, Sitzungsber, 1918: p. 98-100.

50. Liu, Zhen, Wang, Hui, Li, Zengxi, Lu, Xingmei, Zhang, Xiangping, Zhang, Suojiang, and Zhou, Kebin, *Characterization of the regenerated cellulose films in ionic liquids and rheological properties of the solutions.* Materials Chemistry and Physics, 2011. **128**(1–2): p. 220-227.

51. Abdul Khalil, H. P. S., Davoudpour, Y., Islam, Md Nazrul, Mustapha, Asniza, Sudesh, K., Dungani, Rudi, and Jawaid, M., *Production and modification of nanofibrillated cellulose using various mechanical processes: A review.* Carbohydrate Polymers, 2014. **99**: p. 649-665.

52. Kim, Ung-Jin, Park, Jaehyung, Li, Chunmei, Jin, Hyoung-Joon, Valluzzi, Regina, and Kaplan, David L., *Structure and Properties of Silk Hydrogels.* Biomacromolecules, 2004. **5**(3): p. 786-792.

53. Szcześniak, Ludwik, Rachocki, Adam, and Tritt-Goc, Jadwiga, *Glass transition temperature and thermal decomposition of cellulose powder.* Cellulose, 2007. **15**(3): p. 445-451.

54. Um, In Chul, Kweon, HaeYong, Park, Young Hwan, and Hudson, Sam, *Structural characteristics and properties of the regenerated silk fibroin prepared from formic acid.* International Journal of Biological Macromolecules, 2001. **29**(2): p. 91-97.

55. He, Shi-Juang, Valluzzi, Regina, and Gido, Samuel P., *Silk I structure in Bombyx mori silk foams.* International Journal of Biological Macromolecules, 1999. **24**(2–3): p. 187-195.

56. Gong, Zuguang, Huang, Lei, Yang, Yuhong, Chen, Xin, and Shao, Zhengzhong, *Two distinct [small beta]-sheet fibrils from silk protein.* Chemical Communications, 2009(48): p. 7506-7508.

57. Asakura, Tetsuo, Yamane, Tsutomu, Nakazawa, Yasumoto, Kameda, Tsunenori, and Ando, Kazuto, *Structure of Bombyx mori silk fibroin before spinning in solid state studied with wide angle x-ray scattering and 13C cross-polarization/magic angle spinning NMR.* Biopolymers, 2001. **58**(5): p. 521-525.

58. Asakura, Tetsuo, Okushita, Keiko, and Williamson, Mike P., *Analysis of the Structure of Bombyx mori Silk Fibroin by NMR.* Macromolecules, 2015. **48**(8): p. 2345-2357.

59. Liu, Xinfang and Zhang, Ke-Qin, *Silk Fiber—Molecular Formation Mechanism, Structure-Property Relationship and Advanced Applications.* Oligomerization of Chemical and Biological Compounds, 2014. **3**.

60. Saitoh, Hiroyuki, Ohshima, Ken-ichi, Tsubouchi, Kozo, Takasu, Yoko, and Yamada, Hiromi, *X-ray structural study of noncrystalline regenerated Bombyx mori silk fibroin.* International Journal of Biological Macromolecules, 2004. **34**(5): p. 259-265.

61. Vainio, Ulla, Maximova, Natalia, Hortling, Bo, Laine, Janne, Stenius, Per, Simola, Liisa Kaarina, Gravitis, Janis, and Serimaa, Ritva, *Morphology of Dry Lignins and Size and Shape of Dissolved Kraft Lignin Particles by X-ray Scattering.* Langmuir, 2004. **20**(22): p. 9736-9744.

62. Nieduszynski, I and Preston, RD, *Crystallite size in natural cellulose.* Nature, 1970. **225**: p. 273-274.

63. Eyley, Samuel and Thielemans, Wim, *Surface modification of cellulose nanocrystals.* Nanoscale, 2014. **6**(14): p. 7764-7779.

64. French, Alfred D., *Idealized powder diffraction patterns for cellulose polymorphs.* Cellulose, 2014. **21**(2): p. 885-896.

65. Fernandes, Anwesha N, Thomas, Lynne H, Altaner, Clemens M, Callow, Philip, Forsyth, V Trevor, Apperley, David C, Kennedy, Craig J, and Jarvis, Michael C, *Nanostructure of cellulose microfibrils in spruce wood.* Proceedings of the National Academy of Sciences, 2011. **108**(47): p. E1195-E1203.

66. Kafle, Kabindra, Shin, Heenae, Lee, Christopher M, Park, Sunkyu, and Kim, Seong H, *Progressive structural changes of Avicel, bleached softwood, and bacterial cellulose during enzymatic hydrolysis.* Scientific reports, 2015. **5**: p. 1-10.

67. Lewis, Ashley, Waters, Joshua C, Stanton, John, Hess, Joseph, and Salas-de la Cruz, David, *Macromolecular Interactions Control Structural and Thermal Properties of Regenerated Tri-Component Blended Films.* International Journal of Molecular Sciences, 2016. **17**(12): p. 1989.

68. Ibbett, Roger, Gaddipati, Sanyasi, Hill, Sandra, and Tucker, Greg, *Structural reorganisation of cellulose fibrils in hydrothermally deconstructed lignocellulosic biomass and relationships with enzyme digestibility.* Biotechnology for Biofuels, 2013. **6**(1): p. 1-15.

69. Ioelovich, M, *Nano-Structural Approach to Description of Enzymatic Hydrolysis of Pretreated Biomass.* Journal Scientific Israel-Technological Advantages, 2011. **13**(4).

70. Kamel, S, *Nanotechnology and its applications in lignocellulosic composites, a mini review.* Express Polymer Letters, 2007. **1**(9): p. 546-575.

71. Cheng, Gang, Varanasi, Patanjali, Arora, Rohit, Stavila, Vitalie, Simmons, Blake A., Kent, Michael S., and Singh, Seema, *Impact of Ionic Liquid Pretreatment Conditions on Cellulose Crystalline Structure Using 1-Ethyl-3-methylimidazolium Acetate.* The Journal of Physical Chemistry B, 2012. **116**(33): p. 10049-10054.

72. Dammström, Sofia, Salmén, Lennart, and Gatenholm, Paul, *On the interactions between cellulose and xylan, a biomimetic simulation of the hardwood cell wall.* BioResources, 2008. **4**(1): p. 3-14.

73. Busse-Wicher, Marta, Gomes, Thiago CF, Tryfona, Theodora, Nikolovski, Nino, Stott, Katherine, Grantham, Nicholas J, Bolam, David N, Skaf, Munir S, and Dupree, Paul, *The pattern of xylan acetylation suggests xylan may interact with cellulose microfibrils as a twofold helical screw in the secondary plant cell wall of Arabidopsis thaliana.* The Plant Journal, 2014. **79**(3): p. 492-506.

74. Utracki, Leszek A, *Compatibilization of polymer blends.* The Canadian Journal of Chemical Engineering, 2002. **80**(6): p. 1008-1016.

75. Vincent, Julian FV and Wegst, Ulrike GK, *Design and mechanical properties of insect cuticle.* Arthropod structure & development, 2004. **33**(3): p. 187-199.

76. Stanton, John, Xue, Ye, Waters, Joshua C, Lewis, Ashley, Cowan, Darrel, Hu, Xiao, and Salas-de la Cruz, David, *Structure–property relationships of blended polysaccharide and protein biomaterials in ionic liquid.* Cellulose, 2017: p. 1-15.

77. levy, Ilan, Nussinovitch, Amos, Shpigel, Etai, and Shoseyov, Oded, *Recombinant cellulose crosslinking protein: a novel paper-modification biomaterial.* Cellulose. **9**(1): p. 91-98.

78. Swatloski, Richard P., Spear, Scott K., Holbrey, John D., and Rogers, Robin D., *Dissolution of Cellose with Ionic Liquids.* Journal of the American Chemical Society, 2002. **124**(18): p. 4974-4975.

79. Maton, Cedric, De Vos, Nils, and Stevens, Christian V., *Ionic liquid thermal stabilities: decomposition mechanisms and analysis tools.* Chemical Society Reviews, 2013. **42**(13): p. 5963-5977.

80. Pang, Jinhui, Liu, Xin, Zhang, Xueming, Wu, Yuying, and Sun, Runcang, *Fabrication of Cellulose Film with Enhanced Mechanical Properties in Ionic Liquid 1-Allyl-3-methylimidaxolium Chloride (AmimCl).* Materials, 2013. **6**(4): p. 1270-1284.

81. Zhang, Suojiang, Sun, Ning, He, Xuezhong, Lu, Xingmei, and Zhang, Xiangping, *Physical properties of ionic liquids: database and evaluation.* Journal of physical and chemical reference data, 2006. **35**(4): p. 1475-1517.

82. Nazet, Andreas, Sokolov, Sophia, Sonnleitner, Thomas, Makino, Takashi, Kanakubo, Mitsuhiro, and Buchner, Richard, *Densities, Viscosities, and Conductivities of the Imidazolium Ionic Liquids [Emim][Ac], [Emim][FAP], [Bmim][BETI], [Bmim][FSI], [Hmim][TFSI], and [Omim][TFSI].* Journal of Chemical & Engineering Data, 2015. **60**(8): p. 2400-2411.

83. Isik, Mehmet, Sardon, Haritz, and Mecerreyes, David, *Ionic liquids and cellulose: Dissolution, chemical modification and preparation of new cellulosic materials.* International journal of molecular sciences, 2014. **15**(7): p. 11922-11940.

84. Hu, Xiao, Kaplan, David, and Cebe, Peggy, *Determining beta-sheet crystallinity in fibrous proteins by thermal analysis and infrared spectroscopy.* Macromolecules, 2006. **39**(18): p. 6161-6170.

85. Szcześniak, Ludwik, Rachocki, Adam, and Tritt-Goc, Jadwiga, *Glass transition temperature and thermal decomposition of cellulose powder.* Cellulose, 2008. **15**(3): p. 445-451.

86. Jandura, Peter, Riedl, Bernard, and Kokta, Bohuslav V, *Thermal degradation behavior of cellulose fibers partially esterified with some long chain organic acids.* Polymer Degradation and Stability, 2000. **70**(3): p. 387-394.

87. Wang, Fang, Wolf, Nathan, Rocks, Eva-Marie, Vuong, Trinh, and Hu, Xiao, *Comparative studies of regenerated water-based Mori, Thai, Eri, Muga and Tussah silk fibroin films.* Journal of Thermal Analysis and Calorimetry, 2015. **122**(3): p. 1069-1076.